Contents lists available at ScienceDirect

Journal of the Mechanics and Physics of Solids

journal homepage: www.elsevier.com/locate/jmps

A constitutive model for fibrous tissues with cross-linked collagen fibers including dispersion — With an analysis of the Poynting effect

Stephan Teichtmeister [a], Gerhard A. Holzapfel [a,b,*]

[a] Graz University of Technology, Institute of Biomechanics, Austria
[b] Norwegian University of Science and Technology (NTNU), Department of Structural Analysis, Trondheim, Norway

ARTICLE INFO

Keywords:
Hyperelasticity
Collagen fiber
Cross-links
Dispersion
Poynting effect

ABSTRACT

The present work deals with cross-links in collagenous tissues and proposes a planar continuum model for large strains to mechanically characterize, for example, the well-known stiffening effect associated with the presence of these cross-links. A key novelty of the paper is the consideration of dispersed fibers connected by randomly distributed cross-links. The model is essentially based on two mechanisms: (i) a fiber dispersion-induced cross-link dispersion and (ii) a fiber-independent cross-link dispersion connecting two arbitrary parallel fibers of the sample space. Within the framework of the generalized structure tensors, we derive appropriate invariants that enter the stored-energy function, taking into account the stiffness and relative orientation of the cross-links and the cross-link-fiber interaction. To illustrate the power of the proposed model, we first consider uniaxial tension and simple shear. We investigate the influence of different cross-link configurations on the stress response. In particular, we are interested in simple shear and the sign of the normal stress perpendicular to the shear planes, which is referred to as the Poynting effect. We show that the cross-links have a significant impact on the normal stress considered. This may provide a deeper insight into the microstructural mechanisms in semi-flexible biopolymer gels that are responsible for the tendency, in simple shear, of the top and bottom faces to approach each other. Finally, we investigate the Poynting effect that occurs in a circular hollow cylinder under pure torsion, i.e. how the axial normal force correlates with the cross-linked fibrous microstructure of the specimen.

1. Introduction

The mechanical behavior of structural tissues is mainly determined by collagen, an important and abundant protein in the body. Collagen fibers are distributed differently in fibrous tissues, e.g., they are dispersed in arterial walls and nearly parallel in tendons, and can bear considerable mechanical loads, see Fratzl (2008). The hierarchic structure of collagen in particular provides fibrous tissues high toughness and resistance to tensile forces. Amino acids are arranged in a triple helix and form tropocollagen (TC) molecules. Axially staggered arrays of these molecules form collagen fibrils. Within these, TC molecules are connected by intermolecular cross-links, which can be categorized into *enzymatic* and *non-enzymatic* cross-links, see the review articles of Eyre et al. (1984) and Snedeker and Gautieri (2014) whereby the former also provides a chemical background. The origin of non-enzymatic cross-links lies in the reaction of glucose and collagen, through which the advanced glycation end products (AGEs) are built. It is known that this type of cross-links either link neighboring molecules or affect individual proteins. With increasing age and diabetes,

* Corresponding author at: Graz University of Technology, Institute of Biomechanics, Austria.
E-mail address: holzapfel@tugraz.at (G.A. Holzapfel).

https://doi.org/10.1016/j.jmps.2022.104911
Received 18 January 2022; Received in revised form 28 March 2022; Accepted 20 April 2022

the density of these non-enzymatic cross-links in collagen increases over the whole length of the proteins, see, e.g., the review article of Zieman and Kass (2004). This is supposed to change the mechanical behavior of collagenous tissues in the direction of increasing stiffness and brittleness. We also refer to Snedeker and Gautieri (2014) and the references contained therein. On the other hand, cross-links can also be formed by an enzymatic reaction triggered by the protein lysyl oxidase. The result is an immature divalent bond between TC molecules. In contrast to non-enzymatic cross-links, enzymatic cross-links connect TC molecules at their ends. As the tissue ages, these divalent cross-links undergo a further reaction to form a trivalent mature bond that connects three TC molecules and increases collagen interconnectivity and structural stability, see Bailey (2001) for a review. Under a certain monothonic load or with a sufficient number of load cycles, existing cross-links can break and sliding between the filaments is possible, see Willett et al. (2010) and Herod et al. (2016). Normally the cross-links in biomaterials are much weaker than the fibrous structure itself and therefore rupture before the fibers, see Fantner et al. (2006). After unloading, however, a recovery process may take place in the sense that cross-links can be re-established, see Harrington et al. (2009).

In general, the presence of cross-links has a very strong influence on the mechanical behavior of collagenous tissues. High cross-link densities lead to a stronger or more brittle deformation behavior of the tissue due to suppressed intermolecular slip. On the other hand, collagen fibrils, which tend to be poorly cross-linked, show a weaker tensile strength, a reduced tangent modulus and a dissipative deformation character. We refer to the works of Buehler (2008), Depalle et al. (2015) and Yoshida et al. (2014) and the review article of Eekhoff et al. (2018). The influence of the cross-link density on the fracture behavior of fibrous tissues is studied by Svensson et al. (2013). As mentioned above, there is strong evidence that the number of cross-links increases with age, which leads to a change in the biomechanical properties, see the review article of Barodka et al. (2011) on age-related stiffening of the arterial walls or Willett et al. (2010) for a study on tendons. For the chemical mechanisms that lead to an increase in the amount of cross-links between collagen fibrils, we refer to Fujimoto (1982) and Mikšík and Deyl (1991).

Due to the properties mentioned, the mechanics of cross-links has gained a lot of interest also from a theoretical and modeling point of view. In Uzel and Buehler (2011) a fully atomistic model was set up that investigates the influence of covalent cross-links between two type I collagen molecules. The authors come to the conclusion that the influence of cross-links is rather minor for small deformations, but not negligible for large deformations, i.e. the presence of cross-links leads to a significant strengthening, see also Kwansa et al. (2016). In addition, a simple rheological model is proposed in Uzel and Buehler (2011) that is able to reproduce the results of their molecular dynamics simulation, i.e. the elastic, slippage and delayed elastic regimes. Another computational model on the molecular level was recently presented by Shabbir et al. (2019). There, the tensile deformation behavior of parallel fibers, which are connected by two- and three-fold coordinated cross-links, is investigated. It was found that a higher coordination of the cross-links has a positive influence on the strength of the overall fibrous system. In order to analyze the strain stiffening of a biopolymer network in the event of large deformations, Žagar et al. (2015) created a computational random network model from cross-linked fibers. By subjecting the representative volume element to simple shear, they observe the development of localized paths of (highly) axially stressed fibers and cross-links and relate the stiffening of the network to two mechanisms that dominate at large strains, namely their straightening and reorientation of these paths.

Lin and Gu (2015) has also created a model with randomly distributed cross-linked fibers and concluded from their computational tensile tests that an increased cross-link density has a higher influence on the overall stiffness than the cross-link stiffness, see also Chen et al. (2017). The dynamic nature of cross-links in the sense of a changing density in the fibrous material was taken into account in Åström et al. (2008), whereby the cross-links in the random network model can break and reform when the segments come close enough to one another. It is stated that this rebinding forms bunches of tensile-loaded fibers, which leads to a strain stiffening. As an alternative to these network models, Sáez et al. (2014) formulated a continuum-based approach with an isotropic contribution of the cross-links connecting parallel fibers in carotid arteries. The amount of cross-links is controlled by a scalar parameter which is included in the anisotropic stored-energy function, the terms of which model a phase transition of the fiber-related stored energy towards an energy that is associated with cross-links.

In contrast to this, the recent 3D continuum model from Holzapfel and Ogden (2020a) accounts for cross-links via additional structural directors. There, the influence of the cross-link stiffness, the cross-link orientation and the cross-link density on the overall mechanical response of the fibrous tissue for the case of uniaxial deformation and simple shear is studied. The work of Holzapfel and Ogden (2020b) extends this model to a collagen fiber damage formulation with intact cross-links and is embedded in the framework of pseudo-elasticity in the sense of Ogden and Roxburgh (1999). The limitation of these continuum-based models is the assumption of *perfectly aligned* fibers that are connected by cross-links. The purpose of this paper is to develop a *large-strain continuum model*, which now considers *dispersed cross-links* and *dispersed fibers* that are connected by these cross-links. The formulation is essentially based on the deliberation of

(i) a fiber-independent dispersion of cross-links that connect two parallel dispersed fibers and
(ii) a cross-link dispersion which is induced by the dispersion of the fibers.

The presented hyperelastic formulation is embedded within the framework of Generalized Structure Tensors (GST) in the sense of Advani and Tucker III (1987).

One aspect that will be examined in detail in this work concerns the role of cross-links in simple shear deformation. Janmey et al. (2007) have found experimentally that semi-flexible biopolymer gels show a tendency to decrease the distance between parallel shear planes, or in other words, they exhibit a normal tensile stress in the direction perpendicular to the shear planes. This behavior is in contrast to rubber, in which the shear planes have the tendency to spread apart (expand), which is generally known as the *positive Poynting effect*, see Truesdell and Noll (2004). The *negative (or inverse) Poynting effect* in biopolymers observed by Janmey et al. (2007) is supposed to have its origin in network-connecting filaments, which possess a nonlinear force–extension relationship

and thus lead to a net force perpendicular to the shear planes. Conti and MacKintosh (2009) computationally investigated this inverse normal stress effect in a random network model.

From a mathematical and elasticity-theoretical point of view, the sign of the considered normal stress is understood to be governed by material inequalities (e.g., the well-known Baker–Ericksen inequality), which are ultimately formulated for isotropy, see Mihai and Goriely (2011) and the numerical study of Mihai and Goriely (2013), which also discusses generalized shear deformations. Furthermore, it should be noted that in the case of incompressibility, the additional constraint for determining the Lagrange multiplier has a decisive influence on the normal stress behavior as pointed out in Horgan and Murphy (2010). Hence, a compressible formulation for isochoric deformation of simple shear is proposed therein. An analysis of the Poynting effect for transversely isotropic materials undergoing simple shear deformation is given in Horgan and Murphy (2011, 2017) and Destrade et al. (2015).

Note that simple shear is related to the inhomogeneous problem of pure torsion in the sense that *locally* these two deformations are equivalent, see, e.g., Truesdell and Noll (2004). However, as, e.g., pointed out in Horgan and Murphy (2017), torsion produces a characteristically different Poynting effect than that observed in simple shear. Therefore, within the scope of this work, we also investigate the axial normal force generated in a cylindrical specimen under pure torsion, which consists of a cross-linked fibrous material.

The above-mentioned aspects are discussed in detail in the following sections. The novel contributions of the presented work are

- a continuum mechanical model for plane strain deformations, which takes into account both the fiber dispersion and a statistical orientation distribution of fiber-connecting cross-links through the two geometrical mechanisms (i)–(ii) mentioned above,
- the specification of the proposed model for uniaxial extension, simple shear and pure torsion and
- a detailed discussion of the positive/negative Poynting effect in simple shear and pure torsion and how this effect is related to the assumed fiber-cross-link microstructure of the solid.

The paper is organized as follows: In Section 2 we set up the model and start with the description of the microstructure by introducing suitable structure directors. The kinematic basis is the usual multiplicative split of the deformation gradient into volumetric and isochoric parts, but only applied to the isotropic part of the stored-energy function. From a physical point of view, this 'incomplete' split for anisotropy is preferable over the usual 'complete' multiplicative split, which uses the decomposition of the deformation gradient for each part of the stored-energy function, see Sansour (2008). Within the GST approach, we define suitable invariants that take into account the effect of cross-links and the influence of the fiber-cross-link interaction. Finally, we specify the proposed model by assuming a von Mises distribution of the fibers and a von Mises distribution of the cross-links for a fixed fiber direction. In Section 3 we apply the framework to two homogeneous deformation modes, namely uniaxial extension and simple shear, and show the influence of the cross-link dispersion on the stress response. For the latter deformation mode, we will discuss in detail the role of the cross-links concerning the positive/negative Poynting effect, i.e. how the sign of the normal stress under consideration changes depending on the cross-links. Finally, in Section 4 we investigate the Poynting effect in a circular hollow cylinder under pure torsion, i.e. the axial normal force that must occur to sustain the deformation, and its relation to the cross-linked fibrous microstructure.

2. Continuum mechanical framework

2.1. Multiplicative kinematics

We consider a stress-free reference configuration $\mathcal{B}_0 \subset \mathbb{R}^3$ embedded in Euclidean space and denote with $\boldsymbol{\varphi}: \mathcal{B}_0 \to \mathbb{R}^3$ the nonlinear deformation map. The vector-valued function $\boldsymbol{\varphi}$ maps the points $\boldsymbol{X} \in \mathcal{B}_0$ of the reference configuration to the points $\boldsymbol{x} = \boldsymbol{\varphi}(\boldsymbol{X}) \in \mathcal{B}$ of the current configuration $\mathcal{B} \subset \mathbb{R}^3$. In this regard, the deformation gradient $\boldsymbol{F}(\boldsymbol{X}) = \nabla \boldsymbol{\varphi}(\boldsymbol{X})$ must have a positive determinant $\det \boldsymbol{F}(\boldsymbol{X}) > 0$ for all $\boldsymbol{X} \in \mathcal{B}_0$. We also introduce the right and left Cauchy–Green tensor $\boldsymbol{C} = \boldsymbol{F}^T \boldsymbol{F}$ and $\boldsymbol{b} = \boldsymbol{F}\boldsymbol{F}^T$, which play the role of *convected Riemannian metrics* defined on the reference and current configuration, respectively, i.e. these tensors are symmetric and positive definite.

The presented continuum mechanical framework is *partly* based on a multiplicative decomposition

$$\boldsymbol{F} = (J^{1/3}\boldsymbol{1})\overline{\boldsymbol{F}} \tag{1}$$

of the deformation gradient $\boldsymbol{F}$ into a spherical (volumetric) part $J^{1/3}\boldsymbol{1}$ and an unimodular (isochoric) part $\overline{\boldsymbol{F}} = J^{-1/3}\boldsymbol{F}$ with $\det \overline{\boldsymbol{F}} = 1$ by construction, see Simo et al. (1985), Ogden (1997) and Holzapfel (2000) among others. For the material-geometric setting, the decomposition (1) induces

$$\boldsymbol{C} = J^{2/3}\overline{\boldsymbol{C}}, \qquad \overline{\boldsymbol{C}} = \overline{\boldsymbol{F}}^T\overline{\boldsymbol{F}} \tag{2}$$

where $\overline{\boldsymbol{C}}$ is the unimodular part of the right Cauchy–Green tensor.

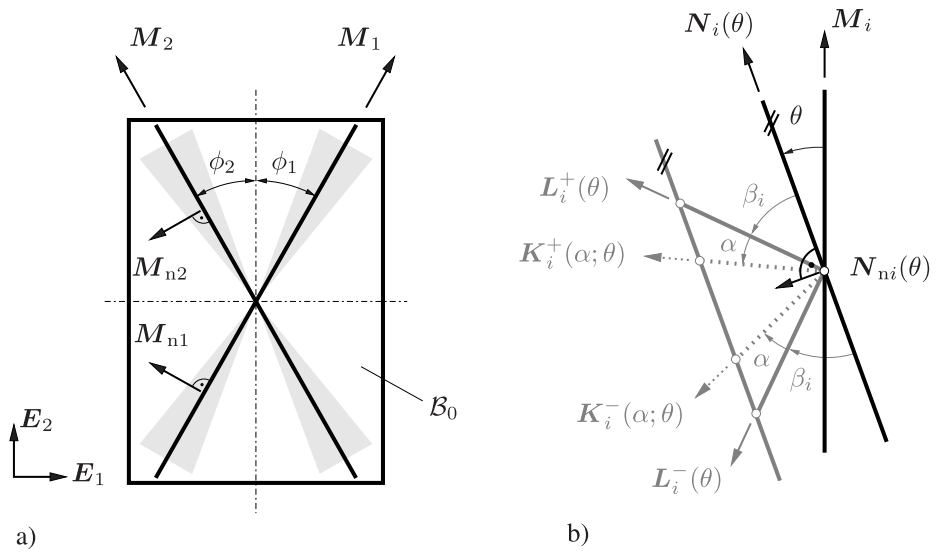

Fig. 1. Geometry of the fiber-cross-link dispersion: (a) two dispersed fiber families with mean unit directions $\boldsymbol{M}_i$ and corresponding normal unit vectors $\boldsymbol{M}_{ni}$, $i = 1, 2$; (b) visualization of the cross-link dispersion with respect to a dispersed fiber direction $\boldsymbol{N}_i(\theta)$. The unit vectors $\boldsymbol{L}_i^{\pm}(\theta)$ denote the mean cross-link directions inclined under a fixed angle $\beta_i \in [0, \frac{\pi}{2}]$ and $\boldsymbol{K}_i^{\pm}(\alpha, \theta)$ the cross-link directions through an additional fiber-independent cross-link dispersion.

2.2. Geometry of planar fiber-cross-link dispersion

Consider a strip of tissue with two dispersed families of fibers, where $\boldsymbol{M}_1$, $\boldsymbol{M}_2$ denote the unit mean directions, see Fig. 1(a). A push forward operation provides the spatial counterparts $\boldsymbol{m}_i = \boldsymbol{F}\boldsymbol{M}_i$, $i = 1, 2$, in the current configuration. We have the component representations

$$[\,\boldsymbol{M}_1\,] = [\,\sin\phi_1,\, \cos\phi_1,\, 0\,]^T\,, \quad [\,\boldsymbol{M}_2\,] = [\,-\sin\phi_2,\, \cos\phi_2,\, 0\,]^T\,, \tag{3}$$

where the two angles ϕ_1, and ϕ_2 are according to Fig. 1(a). It is assumed that the fiber directions do not have an out-of-plane component. Next we consider two parallel and dispersed arbitrary fibers, the directions of which are governed by the unit vector $\boldsymbol{N}_i(\theta)$, where θ denotes the angle between this vector and the mean director $\boldsymbol{M}_i$. Considering the unit normal vector $\boldsymbol{N}_{ni}(\theta)$ for this generic fibers, we can introduce two connecting mean cross-links represented through the unit vectors

$$\boldsymbol{L}_i^{\pm}(\theta) = \pm\cos\beta_i\, \boldsymbol{N}_i(\theta) + \sin\beta_i\, \boldsymbol{N}_{ni}(\theta) \qquad i = 1, 2\,, \tag{4}$$

where we assume a symmetric arrangement of the mean cross-links with respect to $\boldsymbol{N}_{ni}(\theta)$ under the *given* angle $\beta_i \in [0, \frac{\pi}{2}]$, see Fig. 1(b). Finally, we consider dispersed arbitrary cross-links by the unit vectors

$$\boldsymbol{K}_i^{\pm}(\alpha;\theta) = \pm\cos(\beta_i + \alpha)\, \boldsymbol{N}_i(\theta) + \sin(\beta_i + \alpha)\, \boldsymbol{N}_{ni}(\theta)\,, \tag{5}$$

where $\alpha \in [-\beta_i, \frac{\pi}{2} - \beta_i]$ is the angle, measured from the mean cross-link direction $\boldsymbol{L}_i^{\pm}(\theta)$, see again Fig. 1(b). The representations of the directors (4) and (5) with regard to the orthonormal basis system $\boldsymbol{M}_i$, $\boldsymbol{M}_{ni}$ associated with the mean fibers follow from

$$\boldsymbol{N}_i(\theta) = \cos\theta\, \boldsymbol{M}_i + \sin\theta\, \boldsymbol{M}_{ni}\,, \quad \boldsymbol{N}_{ni}(\theta) = -\sin\theta\, \boldsymbol{M}_i + \cos\theta\, \boldsymbol{M}_{ni}\,. \tag{6}$$

Throughout the text, we will make the following additional modeling assumptions:

(i) The deformation is planar, i.e. the out-of-plane axis ($\boldsymbol{E}_3$-direction) is a principal axis with associated principal stretch $\lambda(\boldsymbol{E}_3) = 1$.
(ii) The orientation probability of the cross-links is due to a dispersion of the fibers which are connected by those cross-links and a dispersion that is geometrically independent of the fiber dispersion.
(iii) The dispersion of the fibers is not influenced by the cross-link dispersion.
(iv) The two fiber families and the two cross-link families (for given fiber angle θ) are each equally dispersed and uncoupled.

Based on these assumptions, we will derive generalized structure tensors that govern anisotropic invariants entering the stored-energy function.

2.3. Anisotropic hyperelastic stress response

We consider an additive decomposition of the stored-energy function according to

$$\widehat{\Psi}(\boldsymbol{C};\boldsymbol{M}_1,\boldsymbol{M}_2)=U(J)+\widehat{\Psi}_{\rm iso}(\overline{\boldsymbol{C}})+\widehat{\Psi}_{\rm aniso}(\boldsymbol{C};\boldsymbol{M}_1,\boldsymbol{M}_2) \tag{7}$$

into volumetric, isochoric isotropic and anisotropic parts. Here, $\boldsymbol{M}_1$ and $\boldsymbol{M}_2$ are two material unit vectors that describe the mean directions of two fiber families within the material. Note that within a (weakly) compressible framework, the multiplicative split (2) is *not* applied to the anisotropic part, which would otherwise lead to unphysical stress responses, as outlined in Sansour (2008), Nolan et al. (2014) and Gültekin et al. (2019). The representation theory of scalar-valued tensor functions, see Spencer (1971), Boehler (1987) or Zheng (1994), yields a functional dependence of $\Psi_{\rm iso}$ on two (isochoric) invariants[1] and of $\Psi_{\rm aniso}$ on eight anisotropic invariants

$$\begin{aligned}&\bar{I}_1=\operatorname{tr}\overline{\boldsymbol{C}}\,,\qquad &&\bar{I}_2=\operatorname{tr}[\operatorname{cof}\overline{\boldsymbol{C}}]\,,\quad &&I_{4i}=\boldsymbol{C}:\boldsymbol{H}_i\,,\\ &I_{5i}=\boldsymbol{C}^2:\boldsymbol{H}_i\,,\quad &&I_{6i}=\boldsymbol{C}:\boldsymbol{H}_i^2\,,\quad &&I_{7i}=\boldsymbol{C}^2:\boldsymbol{H}_i^2\end{aligned} \tag{8}$$

where the constant (generalized) structure tensors $\boldsymbol{H}_i$, $i=1,2$, are symmetric $\boldsymbol{H}_i=\boldsymbol{H}_i^T$. If there is no fiber dispersion, the structure tensors have the simple form $\boldsymbol{H}_i=\boldsymbol{M}_i\otimes\boldsymbol{M}_i$, which fulfills the invariance requirement governed by the symmetry group[2] of transverse isotropy $\mathcal{G}_i=\{\,\boldsymbol{R}(\boldsymbol{M}_i,0\le\phi\le2\pi),-\boldsymbol{1}\,\}$. In this case we only get four independent invariants in the anisotropic part $\Psi_{\rm aniso}$ because of $I_{4i}=I_{6i}$ and $I_{5i}=I_{7i}$, where I_{4i} stands for the squared stretch $\lambda^2(\boldsymbol{M}_i)$ in the fiber direction $\boldsymbol{M}_i$. The influence of the cross-links is taken into account by eight additional coupled invariants

$$I_i^{\pm}=\boldsymbol{C}:\boldsymbol{H}_i^{\pm}\,,\qquad I_{8i}^{\star\pm}=\boldsymbol{C}:\boldsymbol{H}_i^{\star\pm}\,, \tag{9}$$

where the constant (generalized) structure tensors $\boldsymbol{H}_i^{\pm}$ and $\boldsymbol{H}_i^{\star\pm}$ are symmetric and model the orientation probability of the cross-links due to fiber dispersion and dispersion that is geometrically independent of the fiber dispersion, see Assumption (ii) in the previous section. In the case of perfectly aligned fibers and cross-links, these tensors should have the form[3]

$$\boldsymbol{H}_i^{\pm}=\boldsymbol{L}_i^{\pm}\otimes\boldsymbol{L}_i^{\pm}\,,\qquad \boldsymbol{H}_i^{\star\pm}=\operatorname{sym}[\,(\boldsymbol{L}_i^{\pm}\otimes\boldsymbol{L}_i^{\pm})(\boldsymbol{M}_i\otimes\boldsymbol{M}_i)\,]\,, \tag{11}$$

where $\boldsymbol{L}_i^{\pm}=\pm\cos\beta_i\,\boldsymbol{M}_i+\sin\beta_i\,\boldsymbol{M}_{{\rm n}i}$. Then $I_i^{\pm}$ represents the squared stretch $\lambda^2(\boldsymbol{L}_i^{\pm})$ in the direction $\boldsymbol{L}_i^{\pm}$ of the cross-links.

For the sake of simplicity we only consider the invariant $\bar{I}_1$ for the isotropic ground substance and only the invariants I_{4i} for the influence of the fibers such that we have the reduced dependencies

$$\Psi_{\rm iso}=\widetilde{\Psi}_{\rm iso}(\bar{I}_1)\quad\text{and}\quad\Psi_{\rm aniso}=\widetilde{\Psi}_{\rm aniso}(I_{4i},I_i^{\pm},I_{8i}^{\star\pm})\,. \tag{12}$$

The stress response of the anisotropic material is

$$\boldsymbol{S}=2\,\partial_{\boldsymbol{C}}\widehat{\Psi}=Jp\boldsymbol{C}^{-1}+\boldsymbol{S}_{\rm iso}+\boldsymbol{S}_{\rm aniso} \tag{13}$$

in terms of the pseudo-pressure[4] $p=U'(J)$, the isochoric isotropic and the anisotropic contribution to the second Piola–Kirchhoff stress tensor is

$$\boldsymbol{S}_{\rm iso}=J^{-2/3}\overline{\boldsymbol{S}}:\mathbb{P}\quad\text{and}\quad\boldsymbol{S}_{\rm aniso}=2\,\partial_{\boldsymbol{C}}\widetilde{\Psi}_{\rm aniso}\,. \tag{14}$$

Herein, $\overline{\boldsymbol{S}}=2\,\partial_{\boldsymbol{C}}\widetilde{\Psi}_{\rm iso}$ is the fictitious isotropic second Piola–Kirchhoff stress tensor and $\mathbb{P}=\mathbb{I}-\frac{1}{3}\,\boldsymbol{C}\otimes\boldsymbol{C}^{-1}$ the fourth-order deviatoric projection tensor in the material setting in terms of the fully symmetric fourth-order unit tensor $\mathbb{I}$, see, e.g., Holzapfel (2000). For incompressible materials $J(\boldsymbol{X})\equiv1$ in $\mathcal{B}_0$, the second Piola–Kirchhoff stress tensor can be written as

$$\boldsymbol{S}=\widetilde{p}\,\boldsymbol{C}^{-1}+2\,(\partial_{\boldsymbol{C}}\widetilde{\Psi}_{\rm iso}+\partial_{\boldsymbol{C}}\widetilde{\Psi}_{\rm aniso}) \tag{15}$$

where the pseudo-pressure $\widetilde{p}$ is a Lagrange multiplier that is not constitutively defined and $\widetilde{\Psi}_{\rm iso}(\cdot)$ coincides with the functional form $(12)_1$, but the argument is replaced by the invariant I_1 built by the right Cauchy–Green tensor $\boldsymbol{C}$.

2.4. Structure tensors accounting for dispersion

With the Generalized Structure Tensor (GST) approach, dispersive effects can be included in the invariant-based formulation (12) of the material model. This averaging approach is based on a distribution density function that characterizes the dispersion of structural directors in relation to unit reference directions, see Advani and Tucker III (1987).

---

[1] The *co-factor* of a second-order tensor $\boldsymbol{A}$ is defined as $\operatorname{cof}\boldsymbol{A}=\boldsymbol{A}^{-T}\det\boldsymbol{A}$

[2] By $\boldsymbol{R}(\boldsymbol{a},\phi)$ we denote a rotation around the $\boldsymbol{a}$-axis by an angle ϕ.

[3] With perfect alignment of fibers and cross-links, an alternative choice for $\boldsymbol{H}_i^{\star\pm}$ would be

$$\boldsymbol{H}_i^{\star\pm}=\operatorname{sym}[\boldsymbol{L}_i^{\pm}\otimes\boldsymbol{M}_i]\,, \tag{10}$$

which, however, is not suitable when it comes to dispersion. We would encounter integrals that, in addition to the cross-link related dispersion parameters defined in (23) and derived from $I_i^{\pm}$, introduce additional dispersion parameters that do not have a closed-form representation.

[4] Since the sum $\boldsymbol{S}_{\rm iso}+\boldsymbol{S}_{\rm aniso}$ of the isochoric isotropic and anisotropic stress contributions is not deviatoric with respect to the metric $\boldsymbol{C}$, the derivative $U'(J)$ cannot be regarded as a hydrostatic pressure.

2.4.1. Fiber dispersion

In the GST approach the structure tensor incorporating fiber dispersion is defined as

$$\boldsymbol{H}_i = \frac{1}{\pi}\int_{-\pi/2}^{\pi/2} \rho_{\mathrm{f}}(\theta)\boldsymbol{N}_i(\theta)\otimes\boldsymbol{N}_i(\theta)\,\mathrm{d}\theta \qquad i=1,2 \tag{16}$$

in terms of a fiber-related probability density function ρ_{f} that fulfills the normalization condition

$$\frac{1}{\pi}\int_{-\pi/2}^{\pi/2} \rho_{\mathrm{f}}(\theta)\,\mathrm{d}\theta = 1\,. \tag{17}$$

In the definition (16) we have already taken into account that a fiber oriented at an angle θ cannot be distinguished from a fiber oriented at $\theta+\pi$. Obviously the generalized structure tensor (16) has the property $\mathrm{tr}\boldsymbol{H}_i = 1$. If the dispersed fibers are symmetrically distributed with respect to the unit reference direction $\boldsymbol{M}_i$, i.e. $\rho_{\mathrm{f}}(\theta) = \rho_{\mathrm{f}}(-\theta)$, we get the representation

$$\boldsymbol{H}_i = \kappa_{\mathrm{f}}\overset{(2)}{\boldsymbol{1}} + (1-2\kappa_{\mathrm{f}})\boldsymbol{M}_i\otimes\boldsymbol{M}_i \quad \text{with} \quad \kappa_{\mathrm{f}} = \frac{1}{\pi}\int_{-\pi/2}^{\pi/2}\rho_{\mathrm{f}}(\theta)\sin^2\theta\,\mathrm{d}\theta \tag{18}$$

being the fiber dispersion parameter, see Gasser et al. (2006) for the general three-dimensional case. Here, $\overset{(2)}{\boldsymbol{1}}$ denotes the *two-dimensional* unit tensor of second order.

2.4.2. Cross-link dispersion

We first consider the dispersion of cross-links connecting parallel fibers that are inclined at a *given* angle θ. Analogous to (16) we define the generalized structure tensor

$$\boldsymbol{G}_i^{\pm}(\theta) = \frac{2}{\pi}\int_{-\beta}^{\frac{\pi}{2}-\beta} \rho_{\mathrm{c}}(\alpha)\boldsymbol{K}_i^{\pm}(\alpha;\theta)\otimes\boldsymbol{K}_i^{\pm}(\alpha;\theta)\,\mathrm{d}\alpha \qquad i=1,2 \tag{19}$$

in terms of a cross-link related probability density function ρ_{c} that fulfills the normalization condition

$$\frac{2}{\pi}\int_{-\beta}^{\frac{\pi}{2}-\beta} \rho_{\mathrm{c}}(\alpha)\,\mathrm{d}\alpha = 1\,. \tag{20}$$

The generalized structure tensor (19) can be written in the form

$$\begin{aligned}\boldsymbol{G}_i^{\pm}(\theta) \;=\; & G_{11}^{\pm}\,\boldsymbol{N}_i(\theta)\otimes\boldsymbol{N}_i(\theta) + G_{22}^{\pm}\,\boldsymbol{N}_{\mathrm{n}i}(\theta)\otimes\boldsymbol{N}_{\mathrm{n}i}(\theta) \\ & + G_{12}^{\pm}\,\boldsymbol{N}_i(\theta)\otimes\boldsymbol{N}_{\mathrm{n}i}(\theta) + G_{21}^{\pm}\,\boldsymbol{N}_{\mathrm{n}i}(\theta)\otimes\boldsymbol{N}_i(\theta)\end{aligned} \tag{21}$$

with the components

$$G_{11}^{\pm} = 1-\widetilde{\kappa}\,, \quad G_{22}^{\pm} = \widetilde{\kappa}\,, \quad G_{12}^{\pm} = G_{21}^{\pm} = \pm\kappa_{\mathrm{c}} \tag{22}$$

in terms of the two cross-link dispersion parameters

$$\widetilde{\kappa} = \frac{2}{\pi}\int_{-\beta}^{\frac{\pi}{2}-\beta}\rho_{\mathrm{c}}(\alpha)\sin^2(\beta+\alpha)\,\mathrm{d}\alpha \quad \text{and} \quad \kappa_{\mathrm{c}} = \frac{2}{\pi}\int_{-\beta}^{\frac{\pi}{2}-\beta}\rho_{\mathrm{c}}(\alpha)\sin(\beta+\alpha)\cos(\beta+\alpha)\,\mathrm{d}\alpha\,. \tag{23}$$

Note that the off-diagonal components are non-zero, i.e. $\kappa_{\mathrm{c}} \neq 0$. With the definitions (23) we can write the structure tensor (19) in the form

$$\boldsymbol{G}_i^{\pm}(\theta) = \widetilde{\kappa}\overset{(2)}{\boldsymbol{1}} + (1-2\widetilde{\kappa})\boldsymbol{N}_i(\theta)\otimes\boldsymbol{N}_i(\theta) \pm 2\kappa_{\mathrm{c}}\,\mathrm{sym}[\boldsymbol{N}_i(\theta)\otimes\boldsymbol{N}_{\mathrm{n}i}(\theta)]\,. \tag{24}$$

Additionally, we mention that with a symmetric distribution of the cross-links with respect to the director $\boldsymbol{L}_i^{\pm}(\theta)$ we have $\beta = \frac{\pi}{4}$ and $\rho_{\mathrm{c}}(\alpha) = \rho_{\mathrm{c}}(-\alpha)$.

2.4.3. $I_i^{\pm}$-Related dispersion

In order to include the influence of the fiber dispersion on the orientation probability of the fiber-connecting cross-links, we need an averaging procedure of the structure tensor $\boldsymbol{G}_i^{\pm}(\theta)$ defined in (19) over the fiber orientation domain. Specifically, the $I_i^{\pm}$-related structure tensor $\boldsymbol{H}_i^{\pm}$ is defined as

$$\boldsymbol{H}_i^{\pm} = \frac{1}{\pi}\int_{-\pi/2}^{\pi/2}\rho_{\mathrm{f}}(\theta)\boldsymbol{G}_i^{\pm}(\theta)\,\mathrm{d}\theta \qquad i=1,2\,. \tag{25}$$

This yields an overall coupled probability density function of the cross-links in a *multiplicative format*, i.e.

$$\rho(\alpha,\theta) = \rho_{\mathrm{c}}(\alpha)\,\rho_{\mathrm{f}}(\theta)\,. \tag{26}$$

Note that we have the property $\mathrm{tr}\boldsymbol{H}_i^{\pm} = 1$ again. For a symmetric distribution of the fibers with respect to the direction $\boldsymbol{M}_i$, we can, by making use of the representations (6), write the structure tensor (25) in the specific form

$$\boldsymbol{H}_i^{\pm} = \widetilde{\kappa}\overset{(2)}{\boldsymbol{1}} + (1-2\widetilde{\kappa})\boldsymbol{H}_i \pm 2\kappa_{\mathrm{c}}(1-2\kappa_{\mathrm{f}})\,\mathrm{sym}[\boldsymbol{M}_i\otimes\boldsymbol{M}_{\mathrm{n}i}] \tag{27}$$

in terms of the dispersion parameters κ_f and $\widetilde{\kappa}$, κ_c defined in $(18)_2$ and (23) and we recall the expression $(18)_1$ for the I_{4i}-related structure tensor $\boldsymbol{H}_i$ accounting for fiber dispersion. We now note some special cases:

- If there is no fiber dispersion, we have $\rho_\mathrm{f}(\theta) = \pi\delta(\theta)$ in terms of the Dirac delta function $\delta(\theta)$ and the dispersion parameter κ_f attains the value $\kappa_\mathrm{f} = 0$. Then, the $I_i^{\pm}$-related structure tensor (27) takes the form (24), but without the functional dependence on θ.
- For a uniform distribution of fibers, we have $\rho_\mathrm{f} = 1$ and the dispersion parameter κ_f attains the value $\kappa_\mathrm{f} = 1/2$. Then we get $\boldsymbol{H}_i^{+} = \boldsymbol{H}_i^{-} = (1/2)\overset{(2)}{\boldsymbol{1}}$ and the invariants $I_i^{+} = I_i^{-}$ are isotropic.
- If there is no fiber-independent cross-link dispersion, we have $\rho_\mathrm{c}(\alpha) = \frac{\pi}{2}\delta(\alpha)$ and the dispersion parameters $\widetilde{\kappa}$ and κ_c have the form

$$\widetilde{\kappa} = \sin^2\beta \quad \text{and} \quad \kappa_\mathrm{c} = \frac{1}{2}\sin(2\beta)\,. \tag{28}$$

  Then $\boldsymbol{G}_i^{\pm}(\theta) = \boldsymbol{L}_i^{\pm}(\theta) \otimes \boldsymbol{L}_i^{\pm}(\theta)$ and the $I_i^{\pm}$-related structure tensor (27) takes for the specific case $\beta = \frac{\pi}{4}$ the form

$$\boldsymbol{H}_i^{\pm} = \frac{1}{2}\overset{(2)}{\boldsymbol{1}} \pm (1-2\kappa_\mathrm{f})\,\mathrm{sym}[\boldsymbol{M}_i \otimes \boldsymbol{M}_{ni}]\,. \tag{29}$$

- Obviously for vanishing cross-links and fiber dispersions, i.e. $\kappa_\mathrm{f} = 0$ and (28) holds, the structure tensor $\boldsymbol{H}_i^{\pm}$ has the standard form $(11)_1$.

2.4.4. $I_{8i}^{\star\pm}$-Related dispersion

In order to consider dispersive effects in the invariant $I_{8i}^{\star\pm}$, we define the generalized structure tensor $\boldsymbol{H}_i^{\star\pm}$ by the following averaging operation on $\boldsymbol{G}_i^{\pm}(\theta)$, i.e.

$$\boldsymbol{H}_i^{\star\pm} = \frac{1}{\pi}\int_{-\pi/2}^{\pi/2} \rho_\mathrm{f}(\theta)\,\mathrm{sym}\{\boldsymbol{G}_i^{\pm}(\theta)[\boldsymbol{N}_i(\theta)\otimes\boldsymbol{N}_i(\theta)]\}\,\mathrm{d}\theta \qquad i = 1,2\,, \tag{30}$$

which again induces the definition of an overall probability density function (26). Note that in contrast to the other structure tensors (16) and (25), $\boldsymbol{H}_i^{\star\pm}$ does, in general, not have the property of the unit trace, i.e. $\mathrm{tr}\boldsymbol{H}_i^{\star\pm} = 1 - \widetilde{\kappa}$. For symmetric fiber dispersions we obtain, after inserting (6) and (24) into (30), the explicit form

$$\boldsymbol{H}_i^{\star\pm} = (1-\widetilde{\kappa})\boldsymbol{H}_i \pm \kappa_\mathrm{c}(1-2\kappa_\mathrm{f})\,\mathrm{sym}[\boldsymbol{M}_i \otimes \boldsymbol{M}_{ni}] \tag{31}$$

in terms of the dispersion parameters κ_f and $\widetilde{\kappa}$, κ_c defined in $(18)_2$ and (23) and where we recall the expression $(18)_1$ for the I_{4i}-related structure tensor $\boldsymbol{H}_i$ accounting for fiber dispersion. Here, too, we would like to point out some special cases:

- If there is no fiber dispersion $\kappa_\mathrm{f} = 0$, the $I_{8i}^{\star\pm}$-related structure tensor (31) becomes

$$\boldsymbol{H}_i^{\star\pm} = \mathrm{sym}[\boldsymbol{G}_i^{\pm}(\boldsymbol{M}_i \otimes \boldsymbol{M}_i)] \tag{32}$$

  in terms of the cross-link dispersion structure tensor (24) without a functional dependence on θ.
- For a uniform distribution of fibers $\kappa_\mathrm{f} = 1/2$, we have $\boldsymbol{H}_i^{\star\pm} = (1/2)(1-\widetilde{\kappa})\overset{(2)}{\boldsymbol{1}}$ and the invariants $I_{8i}^{\star+} = I_{8i}^{\star-}$ are isotropic.
- If no fiber-independent cross-link dispersion is taken into account, i.e. (28) holds, we have $\boldsymbol{G}_i^{\pm}(\theta) = \boldsymbol{L}_i^{\pm}(\theta) \otimes \boldsymbol{L}_i^{\pm}(\theta)$ and the $I_{8i}^{\star\pm}$-related structure tensor (31) reads for the specific case $\beta = \frac{\pi}{4}$

$$\boldsymbol{H}_i^{\star\pm} = \frac{1}{2}\boldsymbol{H}_i \pm \frac{1}{2}(1-2\kappa_\mathrm{f})\,\mathrm{sym}[\boldsymbol{M}_i \otimes \boldsymbol{M}_{ni}]\,. \tag{33}$$

- Apparently, for vanishing cross-link and fiber dispersions, i.e. $\kappa_\mathrm{f} = 0$ and (28) holds, the structure tensor $\boldsymbol{H}_i^{\star\pm}$ takes the standard form $(11)_2$.

Finally it should be noted that the maybe more intuitive choice $\mathrm{sym}[\boldsymbol{H}_i^{\pm}\boldsymbol{H}_i]$ for the $I_{8i}^{\star\pm}$-related structure tensor does not work due to the *unilateral* geometric coupling of the cross-links and the fiber dispersion, see Assumption (iii) in Section 2.2.

2.5. Dispersion parameters for the von Mises distribution

To describe the (symmetric) probability distribution of fibers, it has been found proper to use the von Mises distribution, i.e. the probability density function ρ_f is specified as

$$\rho_\mathrm{f}(\theta) = \frac{1}{I_0(a)}\,\exp[a\cos(2\theta)] \tag{34}$$

in terms of a concentration parameter a and the modified Bessel function $I_0(a)$ of the first kind of order zero. Analogously, we assume for a fixed fiber angle θ a von Mises distribution of the cross-links with $\beta = \pi/4$ such that the probability density function ρ_c reads

$$\rho_\mathrm{c}(\alpha) = \frac{1}{I_0(b)}\,\exp[b\cos(4\alpha)]\,, \tag{35}$$

where b is again a concentration parameter. These two functions specify the overall probability density function (26).

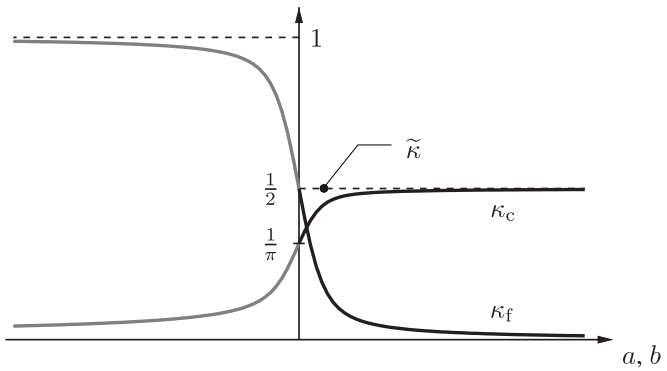

Fig. 2. Dispersion parameters: we observe the ranges $0 \leq \kappa_f \leq 1$ and $0 \leq \kappa_c \leq 1/2$, where only the values corresponding to non-negative concentration parameters a, b (marked as black solid curves) retain the meaning of the directors $\boldsymbol{M}_i$, $\boldsymbol{L}_i^{\pm}$ as mean fiber and cross-link directions, respectively.

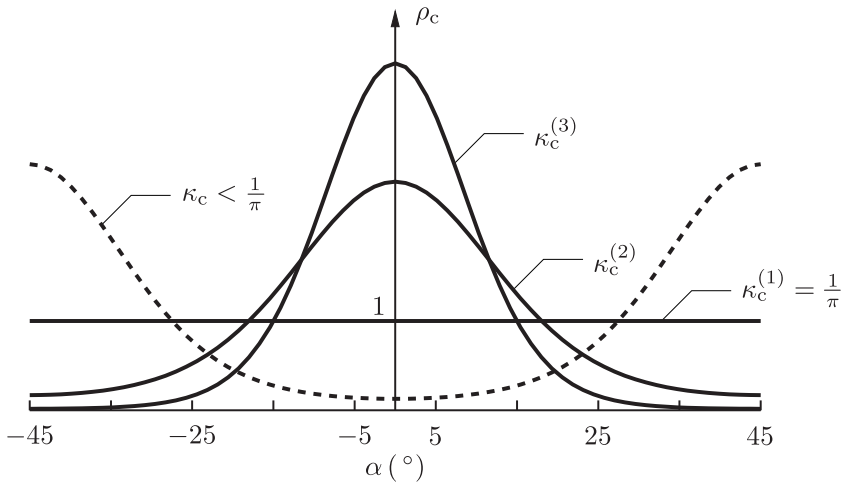

Fig. 3. Cross-link probability density function: von Mises distribution (35) for different values of the dispersion parameters $1/\pi = \kappa_c^{(1)} < \kappa_c^{(2)} < \kappa_c^{(3)}$. For the dispersion parameters $\kappa_c < 1/\pi$ (or equivalently $b < 0$), the function localizes at the ends of the domain and the directors $\boldsymbol{L}_i^{\pm}$ lose the meaning of mean cross-link directions.

The dispersion parameters κ_f and $\widetilde{\kappa}$, κ_c defined in $(18)_2$ and (23), result into

$$\kappa_f = \frac{I_0(a) - I_1(a)}{2I_0(a)} \quad \text{and} \quad \widetilde{\kappa} = \frac{1}{2}\,, \quad \kappa_c = \frac{\exp(b)\,\mathrm{erf}(\sqrt{2b})}{2\sqrt{2\pi b}\,I_0(b)} \tag{36}$$

in terms of the modified Bessel function $I_1(a)$ of the first kind of order one and the standard error function

$$\mathrm{erf}(x) = \frac{2}{\sqrt{\pi}} \int_0^x \exp(-y^2)\,\mathrm{d}y\,. \tag{37}$$

The functions (36) are shown in Fig. 2. Note that because of $\widetilde{\kappa} = 1/2$ the second term in the structure tensor (27) vanishes and the coupling only occurs via the off-diagonal terms. In addition, the trace of the structure tensor (25) becomes $\mathrm{tr}\boldsymbol{H}_i^{\star\pm} = 1/2$. According to $(36)_1$, the fiber dispersion parameter κ_f is in the range $\kappa_f \in [\,0, 1/2\,]$, where the lower bound ($a \to \infty$) corresponds to an ideal fiber alignment in the direction $\boldsymbol{M}_i$ and the upper bound ($a \to 0$) to a uniform fiber distribution. Mathematically, negative concentration parameters a are possible, but lead to probability density functions that are localized at the ends $\theta = \pm\pi/2$ and the normal vectors $\boldsymbol{M}_{ni}$ take on the role of the mean fiber directors. For the cross-link dispersion parameter κ_c in $(36)_3$ we find the admissible range $\kappa_c \in [\,1/\pi, 1/2\,]$, where for a given fiber angle, the lower bound ($b \to 0$) models a distribution of cross-links that is uniform over the quarter circle and the upper bound ($b \to \infty$) an ideal alignment of cross-links. Again, negative values of the concentration parameter b are possible, but the vectors $\boldsymbol{L}_i^{\pm}$ lose the meaning of mean cross-link directions, see Fig. 3.

2.6. Specification of the stored-energy function

We now specify the anisotropic stress response of a tissue with dispersed fibers connected by cross-links. The isochoric isotropic part $(12)_1$ is related to the ground substance and the anisotropic part $(12)_2$ takes into account the mechanical responses of the fibers, the cross-links and the cross-link-fiber interaction, i.e.

$$\widetilde{\Psi}_{\rm iso}(\bar{I}_1) = \widetilde{\Psi}_{\rm g}(\bar{I}_1) \quad \text{and} \quad \widetilde{\Psi}_{\rm aniso}(I_{4i}, I_i^{\pm}, I_{8i}^{\star\pm}) = \sum_{i=1,2} [\, \widetilde{\Psi}_{\rm f}(I_{4i}) + \widetilde{\Psi}_{\rm c}(I_i^{\pm}) + \widetilde{\Psi}_{\rm fc}(I_{8i}^{\star\pm}) \,] \,. \tag{38}$$

The contributions from the isotropic ground substance and the fibers are specified by a neo-Hookean function and the model of Holzapfel et al. (2000) to give

$$\widetilde{\Psi}_{\rm g}(\bar{I}_1) = \frac{1}{2}\,\mu(\bar{I}_1 - 3) \quad \text{and} \quad \widetilde{\Psi}_{\rm f}(I_{4i}) = \frac{k_1}{2k_2}\{\, \exp[\, k_2(I_{4i}-1)^2\,] - 1\,\} \tag{39}$$

in terms of the shear modulus $\mu > 0$, the stress-like constant $k_1 > 0$ and the dimensionless constant $k_2 > 0$. The influence of the cross-links and the fiber-cross-link interaction on the mechanical behavior are modeled by the stored-energy functions

$$\widetilde{\Psi}_{\rm c}(I_i^{\pm}) = \frac{1}{2}\,\nu(I_i^{\pm} - 1)^2 \quad \text{and} \quad \widetilde{\Psi}_{\rm fc}(I_{8i}^{\star\pm}) = \frac{1}{2}\,c(I_{8i}^{\star\pm} - 1 + \widetilde{\kappa})^2 \tag{40}$$

in terms of the material parameters $\nu \geq 0$ and $c \geq 0$ which measure the stiffness of the cross-links and the strength of the fiber-cross-link connection, respectively.[5] Then, the anisotropic contribution $(14)_2$ to the second Piola–Kirchhoff stress tensor is of the specific form

$$\begin{aligned} \boldsymbol{S}_{\rm aniso} \;=\; & \sum_{i=1,2} \{\, 2\kappa_{\rm f}\, \widetilde{\Psi}'_{\rm f}(I_{4i}) + 2[\,\widetilde{\kappa} + \kappa_{\rm f}(1-2\widetilde{\kappa})\,]A_i^{+} + 2\kappa_{\rm f}(1-\widetilde{\kappa})B_i^{+}\,\}^{(2)}\boldsymbol{1} \\ & + \sum_{i=1,2} 2(1-2\kappa_{\rm f})[\,\widetilde{\Psi}'_{\rm f}(I_{4i}) + (1-2\widetilde{\kappa})A_i^{+} + (1-\widetilde{\kappa})B_i^{+}\,]\boldsymbol{M}_i \otimes \boldsymbol{M}_i \\ & + \sum_{i=1,2} 2\kappa_{\rm c}(1-2\kappa_{\rm f})(2A_i^{-} + B_i^{-})\,\mathrm{sym}[\boldsymbol{M}_i \otimes \boldsymbol{M}_{{\rm n}i}] \end{aligned} \tag{42}$$

with the abbreviations

$$A_i^{\pm} = \widetilde{\Psi}'_{\rm c}(I_i^{+}) \pm \widetilde{\Psi}'_{\rm c}(I_i^{-}) \quad \text{and} \quad B_i^{\pm} = \widetilde{\Psi}'_{\rm fc}(I_{8i}^{\star+}) \pm \widetilde{\Psi}'_{\rm fc}(I_{8i}^{\star-}) \,, \tag{43}$$

where $(\cdot)'$ denotes the ordinary derivative of the function with respect to its argument.

3. Homogeneous examples

We now apply the proposed model to two homogeneous deformation modes, namely uniaxial extension and simple shear. We assume vanishing volume forces and neglect inertia, so that the balance of linear momentum $\mathrm{Div}(\boldsymbol{F}\boldsymbol{S}) = \boldsymbol{0}$ is satisfied. The compatibility condition $\mathrm{Curl}^T \boldsymbol{F} = \boldsymbol{0}$ is trivially fulfilled.

3.1. Uniaxial extension

As a first model problem, we consider a tissue with one symmetrically dispersed fiber family that is extended by a stretch $\lambda \geq 1$ in the direction $\boldsymbol{M}$ of the mean fiber such that[6]

$$\boldsymbol{F}\boldsymbol{M} = \lambda \boldsymbol{M} \quad \text{and} \quad \boldsymbol{F}\boldsymbol{M}_{\rm n} = \lambda^{-1}\boldsymbol{M}_{\rm n} \,. \tag{44}$$

We assume that the material is incompressible and the governing invariants are built by the right Cauchy–Green tensor $\boldsymbol{C}$. The kinematics (44) results in $I^{+} = I^{-}$ and $I_8^{\star+} = I_8^{\star-}$ and consequently $A^{+} = 2\widetilde{\Psi}'_{\rm c}(I^{+})$, $A^{-} = 0$ and $B^{+} = 2\widetilde{\Psi}'_{\rm fc}(I_8^{\star+})$, $B^{-} = 0$. We assume that the dispersion of the cross-links is only induced by the dispersion of the fibers. Then the dispersion parameters $\widetilde{\kappa}$ and $\kappa_{\rm c}$ (only $\widetilde{\kappa}$ is relevant here) in terms of the angle β take the form (28), which describes the orientation of the cross-links with respect to the parallel fibers connecting them, see Fig. 1(b). The anisotropic invariants take the specific forms

$$I_4 \;=\; \kappa_{\rm f}\lambda^{-2} + (1-\kappa_{\rm f})\lambda^{2} \,, \tag{45}$$

$$I^{+} = I^{-} \;=\; \frac{1}{2}(\lambda^{-2} - \lambda^{2})[\,1 - (1-2\kappa_{\rm f})\cos 2\beta\,] + \lambda^{2} \,, \tag{46}$$

---

[5] **Fiber and Cross-Link Density.** For simplicity, we did not explicitly consider the volume fractions of fibers and cross-links. However, this can easily be achieved by modifying (38) in this way

$$\Psi = [\,1 - \sum_{i=1,2}(\phi_{{\rm f}i} + \phi_{{\rm c}i})\,]\,\widetilde{\Psi}_{\rm g}(\bar{I}_1) + \sum_{i=1,2}\{\,\phi_{{\rm f}i}\,\widetilde{\Psi}_{\rm f}(I_{4i}) + \phi_{{\rm c}i}\,[\,\widetilde{\Psi}_{\rm c}(I_i^{\pm}) + \widetilde{\Psi}_{\rm fc}(I_{8i}^{\star\pm})\,]\,\} \,, \tag{41}$$

where $\phi_{{\rm f}i}$, $\phi_{{\rm c}i} \in [0,1]$ with $\max\{\,\sum_{i=1,2}(\phi_{{\rm f}i} + \phi_{{\rm c}i})\,\} = 1$ are the fractions of the fibers and cross-links per unit undeformed volume associated with fiber family i.

[6] Recall Assumption (i) of plane strain, specified in Section 2.2.

$$I_8^{\star+} = I_8^{\star-} = [\,\kappa_\mathrm{f}\lambda^{-2} + (1-\kappa_\mathrm{f})\lambda^2\,]\cos^2\beta\,, \tag{47}$$

and we observe $I_8^{\star+} = I_8^{\star-} = I_4\cos^2\beta$. A push-forward of the second Piola–Kirchhoff stress tensor (15) yields the Cauchy stress tensor

$$\begin{aligned}\boldsymbol{\sigma} = \widetilde{p}\boldsymbol{1} \;+\; \mu\boldsymbol{b} + \{\,2\kappa_\mathrm{f}\,\widetilde{\Psi}_\mathrm{f}'(I_4) + \kappa_\mathrm{f}B^+ + A^+ + [\,\kappa_\mathrm{f}B^+ - (1-2\kappa_\mathrm{f})A^+\,]\cos 2\beta\,\}\overset{(2)}{\boldsymbol{b}} \\ +\; (1-2\kappa_\mathrm{f})[\,2\widetilde{\Psi}_\mathrm{f}'(I_4) + B^+ + (B^+ + 2A^+)\cos 2\beta\,]\,\lambda^2\boldsymbol{M}\otimes\boldsymbol{M}\end{aligned} \tag{48}$$

in terms of the two- and three-dimensional left Cauchy–Green tensor

$$\overset{(2)}{\boldsymbol{b}} = \lambda^2\boldsymbol{M}\otimes\boldsymbol{M} + \lambda^{-2}\boldsymbol{M}_\mathrm{n}\otimes\boldsymbol{M}_\mathrm{n} \quad\text{and}\quad \boldsymbol{b} = \overset{(2)}{\boldsymbol{b}} + \boldsymbol{E}_3\otimes\boldsymbol{E}_3\,, \tag{49}$$

which have the same form as the two- and three-dimensional right Cauchy–Green tensor, respectively. Additionally we have the expressions

$$A^+ = 2v(I^+ - 1) \quad\text{and}\quad B^+ = 2c(I_8^{\star+} - \cos^2\beta)\,. \tag{50}$$

The Lagrange multiplier $\widetilde{p}$ can be determined by a condition of vanishing normal stress in the lateral direction $\boldsymbol{M}_\mathrm{n}$, i.e.

$$\widetilde{p} = -\{\,\mu + 2\kappa_\mathrm{f}\,\widetilde{\Psi}_\mathrm{f}'(I_4) + \kappa_\mathrm{f}B^+ + A^+ + [\,\kappa_\mathrm{f}B^+ - (1-2\kappa_\mathrm{f})A^+\,]\cos 2\beta\,\}\lambda^{-2}\,. \tag{51}$$

Then the normal Cauchy stress in the mean fiber direction $\boldsymbol{M}$ takes on the final form

$$\begin{aligned}\sigma \;=\; \lambda^2\{\,\mu + A^+ + (1-\kappa_\mathrm{f})[\,2\widetilde{\Psi}_\mathrm{f}'(I_4) + B^+\,] + [\,\kappa_\mathrm{f}B^+ + (1-2\kappa_\mathrm{f})(A^+ + B^+)\,]\cos 2\beta\} \\ -\,\lambda^{-2}\{\,\mu + 2\kappa_\mathrm{f}\,\widetilde{\Psi}_\mathrm{f}'(I_4) + \kappa_\mathrm{f}B^+ + A^+ + [\,\kappa_\mathrm{f}B^+ - (1-2\kappa_\mathrm{f})A^+\,]\cos 2\beta\,\}\,.\end{aligned} \tag{52}$$

Based on this expression, we investigate the stress response for two different orientations of the cross-links as shown in Fig. 4.

For $\beta = 90°$ the cross-links are orthogonal to the dispersed fibers and the expression (52) for the normal stress reduces to

$$\sigma = \mu(\lambda^2 - \lambda^{-2}) + 2\lambda^2[\,(1-\kappa_\mathrm{f})\widetilde{\Psi}_\mathrm{f}'(I_4) + \kappa_\mathrm{f}\,A^+\,] - 2\lambda^{-2}[\,\kappa_\mathrm{f}\,\widetilde{\Psi}_\mathrm{f}'(I_4) + (1-\kappa_\mathrm{f})A^+\,]\,. \tag{53}$$

We observe that the strength of the cross-link-fiber interaction is irrelevant for the normal stress in the mean fiber direction, i.e. σ is not a function of B^+ since $I_8^{\star\pm} = 0$. The sensitivity with respect to the cross-link stiffness reads

$$\frac{\partial\sigma}{\partial v} = 4(I^+ - 1)[\,\kappa_\mathrm{f}\lambda^2 - (1-\kappa_\mathrm{f})\lambda^{-2}\,] \tag{54}$$

which, depending on the fiber dispersion parameter κ_f, can switch the sign during tensile loading. For $\kappa_\mathrm{f} = 0$, however, we get a non-negative sensitivity $\partial\sigma/\partial v = 4\lambda^{-4}(\lambda^2 - 1) \geq 0$, i.e. the presence of cross-links leads to an overall stiffer response, as reported in Holzapfel and Ogden (2020a). We now specify the dimensionless material parameters as $\bar{k}_1 = k_1/\mu = 1$, $k_2 = 0.3$ and $\bar{v} = v/\mu = 5$. From the solid curves in Fig. 4(a) it can be seen that an increasing value of κ_f leads to a certain reduction in the (global) stiffness.[7] We do not have a continuous decrease of the (global) stiffness with increasing fiber dispersion parameter, as indicated by the dashed curves in Fig. 4(a). This is because the more dispersed the fibers become, the closer the cross-links are to the loading direction, resulting in an increase of the (global) stiffness.

Next, we investigate a cross-link orientation of $\beta = 30°$. The values of the dimensionless material parameters $\bar{k}_1$, k_2 and $\bar{v}$ are the same as before and we additionally set $\bar{c} = c/\mu = 0$. The corresponding stress response for different values of κ_f can be observed from the solid curves in Fig. 4(b). We recognize a decreasing (global) stiffness for increasing values of the fiber dispersion parameter up to the final value $\kappa_\mathrm{f} = 1/2$. This is in contrast to the previous case $\beta = 90°$ since at cross-link orientation $\beta = 30°$, the stiffest configuration is achieved for fibers perfectly aligned to the tensile loading direction. This observation can be roughly generalized for the considered model problem of uniaxial extension: for cross-link topologies with a (more or less) acute angle β, the (global) stiffness continuously decreases with increasing fiber dispersion parameter κ_f, while for cross-link topologies with a (more or less) obtuse angle β, we expect an increase in (global) stiffness if the fibers are sufficiently dispersed. Finally, to show the general stiffening influence of the cross-links, the dotted curves in Fig. 4(b) correspond to a stress response without cross-links ($\bar{v} = 0$).

---

[7] **Global versus Local Stiffness.** If we denote by $\boldsymbol{t}$ the true traction vector in the loading direction $\boldsymbol{M}$, we write $\boldsymbol{t} = (\sigma/\lambda)\,\lambda_{\boldsymbol{M}}$, where $\lambda_{\boldsymbol{M}}$ is the corresponding spatial stretch vector. Building the total differential yields

$$\mathrm{d}\boldsymbol{t} = \boldsymbol{K}_T\,\mathrm{d}\lambda_{\boldsymbol{M}} \quad\text{with}\quad \boldsymbol{K}_T = \frac{1}{\lambda^2}\left(\frac{\mathrm{d}\sigma}{\mathrm{d}\lambda} - \frac{\sigma}{\lambda}\right)\lambda_{\boldsymbol{M}}\otimes\lambda_{\boldsymbol{M}} + \frac{\sigma}{\lambda}\boldsymbol{1}\,, \tag{55}$$

where $\boldsymbol{K}_T$ is the stiffness tensor. Decomposition of the infinitesimal stretch vector $\mathrm{d}\lambda_{\boldsymbol{M}} = \mathrm{d}\lambda\,\boldsymbol{M} + \mathrm{d}\gamma\,\boldsymbol{M}_\mathrm{n}$, where $\mathrm{d}\lambda$ is an infinitesimal stretch in direction $\boldsymbol{M}$ and $\mathrm{d}\gamma$ is an amount of shear related to an infinitesimal simple shear deformation in direction $\boldsymbol{M}_n$, we obtain the separate traction increments from (55)

$$\mathrm{d}\boldsymbol{t}^{\parallel} = \frac{\mathrm{d}\sigma}{\mathrm{d}\lambda}\,\mathrm{d}\lambda\,\boldsymbol{M} \quad\text{and}\quad \mathrm{d}\boldsymbol{t}^{\perp} = \frac{\sigma}{\lambda}\,\mathrm{d}\gamma\,\boldsymbol{M}_\mathrm{n}\,. \tag{56}$$

From there we see that increments of stretch and simple shear lead to different increments in the traction governed by the local (or differential) stiffness $\mathrm{d}\sigma/\mathrm{d}\lambda$ and the factor σ/λ, which represents the global stiffness multiplied with $1 - 1/\lambda$, respectively.

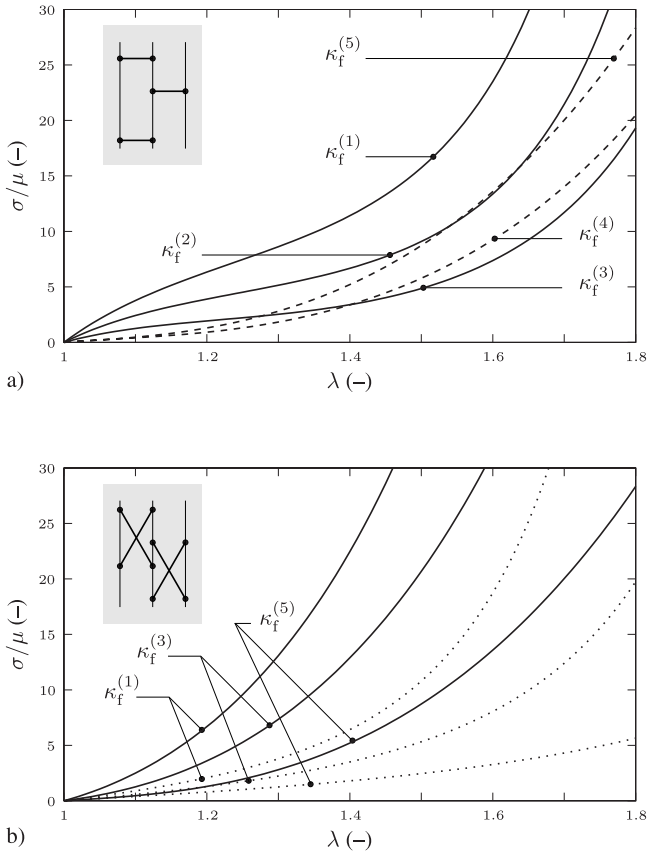

Fig. 4. Uniaxial extension: stress response for cross-link orientations (a) $\beta = 90°$ and (b) $\beta = 30°$ at different values of the fiber dispersion parameter $\kappa_f^{(1)} = 0$ (ideal fiber alignment), $\kappa_f^{(2)} = 0.1$, $\kappa_f^{(3)} = 0.22$, $\kappa_f^{(4)} = 0.42$ and $\kappa_f^{(5)} = 0.5$ (uniform fiber distribution). The other material parameters are chosen as $\bar{k}_1 = k_1/\mu = 1$, $k_2 = 0.3$, $\bar{\nu} = \nu/\mu = 5$ and $\bar{c} = c/\mu = 0$. The solid/dashed curves in (a) indicate a decrease/increase of the (global) stiffness for increasing fiber dispersion parameter. In (b) the dotted curves correspond to different values of κ_f without cross-links ($\bar{\nu} = 0$).

3.2. Simple shear and the Poynting effect

As a second homogeneous model problem, we consider simple shear and refer again to Fig. 1(a). It is assumed that the tissue has only one symmetrically dispersed fiber family and we write $\boldsymbol{M} = \boldsymbol{M}_1$ and $\phi = \phi_1$. The deformation gradient has the specific form $\boldsymbol{F} = \boldsymbol{1} + \gamma \boldsymbol{E}_1 \otimes \boldsymbol{E}_2$, in terms of the amount of shear $\gamma \geq 0$. The push-forwards of the structural director and its normal are as follows

$$\boldsymbol{m} = \boldsymbol{M} + \gamma \cos\phi \, \boldsymbol{E}_1 \quad \text{and} \quad \boldsymbol{m}_n = \boldsymbol{M}_n + \gamma \sin\phi \, \boldsymbol{E}_1 \, . \tag{57}$$

We take the range $\phi \in [0, \pi/2]$ in such a way that the mean fiber is always extended $\lambda(\boldsymbol{M}) \geq 1$. As will be explained later, we assume that the material is *nearly incompressible*. Therefore, we apply the volumetric–isochoric split of the deformation gradient on the isotropic part of the stored-energy function, but *not* on the anisotropic part, as indicated in (12). A reason for such an 'incomplete' split will be given in Section 3.2.1. We fix the orientation of the mean cross-links with respect to the fibers connecting them to $\beta = 45°$ and consider the fiber-independent symmetric cross-link dispersion governed by the parameters $\widetilde{\kappa} = 1/2$ and κ_c specified in $(36)_{2-3}$. The invariants take the specific forms

$$I_1 = 3 + \gamma^2 \, , \tag{58}$$

$$I_4 = \frac{1}{2}[\, 2 + \gamma^2 + \gamma(1 - 2\kappa_f)(\gamma \cos 2\phi + 2 \sin 2\phi) \,] \, , \tag{59}$$

$$I^{\pm} = \frac{1}{2}[\, 2 + \gamma^2 \pm 2\gamma\kappa_c(1 - 2\kappa_f)(\gamma \sin 2\phi - 2 \cos 2\phi) \,] \, , \tag{60}$$

$$I_8^{\star\pm} = \frac{1}{2}[\, I_4 \pm \gamma\kappa_c(1 - 2\kappa_f)(\gamma \sin 2\phi - 2 \cos 2\phi) \,] \, , \tag{61}$$

where $\bar{I}_1 = I_1$ due to the isochoric deformation mode. A push-forward of the second Piola–Kirchhoff stress tensor (13) gives the Cauchy stress tensor

$$\begin{aligned}\boldsymbol{\sigma} &= -\frac{\mu}{3} I_1 \boldsymbol{1} + \mu \boldsymbol{b} + [\, 2\kappa_\mathrm{f} \widetilde{\Psi}'_\mathrm{f}(I_4) + A^+ + \kappa_\mathrm{f} B^+ \,] \overset{(2)}{\boldsymbol{b}} \\ &\quad + (1-2\kappa_\mathrm{f})[\, 2\widetilde{\Psi}'_\mathrm{f}(I_4) + B^+ \,] \boldsymbol{m} \otimes \boldsymbol{m} + 2\kappa_\mathrm{c}(1-2\kappa_\mathrm{f})(2A^- + B^-)\, \mathrm{sym}[\boldsymbol{m} \otimes \boldsymbol{m}_\mathrm{n}]\end{aligned} \tag{62}$$

in terms of the two- and three-dimensional left Cauchy–Green tensor

$$\overset{(2)}{\boldsymbol{b}} = \overset{(2)}{\boldsymbol{1}} + \gamma^2 \boldsymbol{E}_1 \otimes \boldsymbol{E}_1 + 2\gamma\, \mathrm{sym}[\boldsymbol{E}_1 \otimes \boldsymbol{E}_2] \quad \text{and} \quad \boldsymbol{b} = \overset{(2)}{\boldsymbol{b}} + \boldsymbol{E}_3 \otimes \boldsymbol{E}_3 \,. \tag{63}$$

Additionally, we have the expressions

$$\begin{aligned} A^+ &= \nu(I^+ + I^- - 2)\,, \qquad A^- = \nu(I^+ - I^-)\,, \\ B^+ &= c(I_8^{\star +} + I_8^{\star -} - 1)\,, \quad B^- = c(I_8^{\star +} - I_8^{\star -})\,. \end{aligned} \tag{64}$$

Inserting (60) and (61) we see that $A^+ = \nu\gamma^2$ and $B^+ = c(I_4 - 1)$ are independent of the dispersion parameter κ_c. Note that due to the isochoric deformation mode, the volumetric stored-energy function $U(J)$ does not play a role since $U'(1) = 0$, i.e. the stresses are independent of the bulk modulus K. Hence, the incompressible limit[8] cannot be obtained from (62) by taking $K \to \infty$. In this simple shear example we are interested in the normal stress σ_{22} in the direction perpendicular to the shear planes (lateral direction). In particular, we want to know under what conditions this stress is compressive (the body wants to expand laterally) or tensile (the body wants to shrink laterally). From (62) we obtain

$$\begin{aligned}\sigma_{22} &= -\frac{\mu}{3}(3+\gamma^2) + \mu + 2\kappa_\mathrm{f}\widetilde{\Psi}'_\mathrm{f}(I_4) + A^+ + \kappa_\mathrm{f} B^+ + (1-2\kappa_\mathrm{f})[\, 2\widetilde{\Psi}'_\mathrm{f}(I_4) + B^+ \,]\cos^2\phi \\ &\quad + \kappa_\mathrm{c}(1-2\kappa_\mathrm{f})(2A^- + B^-)\sin 2\phi\,.\end{aligned} \tag{68}$$

Experimentally it was observed by Poynting (1909) that elastic rods made out of rubber usually extend along their axis when twisted, which is called the *positive* Poynting effect. In case of simple shear, this scenario roughly translates into the tendency for the specimen to spread apart at the top and bottom. It is important to note that the *local* kinematic equivalence of pure torsion with simple shear does not necessarily result in the same characteristic Poynting effect, which requires a separate analysis for pure torsion. This is discussed in detail in Section 4.

In contrast, semi-flexible biopolymer gels exhibit the behavior of approaching top and bottom faces under simple shear. This is called the *negative* Poynting effect and was observed experimentally[9] by Janmey et al. (2007) and Kang et al. (2009). The explanation for this opposite effect in biopolymeric gels is believed to be that the *network connecting* filaments cause a net tension in the direction orthogonal to the shear planes. Starting with the expression (68) for the lateral normal stress necessary to maintain the simple shear deformation, let us now examine both the positive and negative Poynting effects and their relationship to cross-links, fiber and cross-link dispersion. Before we proceed by considering different orientations of the mean fibers, we put a remark concerning simple shear.

Remark. A problem encountered with simple shear is that it is quite difficult to experimentally realize its kinematic conditions. More realistic problems such as double lap shear should therefore be taken into account in the future via FE computations.

3.2.1. Horizontal mean fiber direction

We consider the case of horizontal mean fibers $\phi = 90°$ (which are not subject to stretching) and simplify the expression (68) to

$$\sigma_{22} = -\frac{\mu}{3}\gamma^2 + 2\kappa_\mathrm{f}\widetilde{\Psi}'_\mathrm{f}(I_4) + A^+ + \kappa_\mathrm{f} B^+ \,. \tag{69}$$

We observe immediately that this stress is independent of the fiber-independent dispersion of the cross-links, i.e. it is not a function of the parameter κ_c.

---

[8] **Compressibility and Incompressibility for Isochoric Deformation.** Recalling stress (13) for a compressible material together with the definitions (14), we obtain for an isochoric deformation

$$\boldsymbol{S} = [\, p - \frac{1}{3}(\overline{\boldsymbol{S}} : \boldsymbol{C})\,]\boldsymbol{C}^{-1} + \overline{\boldsymbol{S}} + 2\,\partial_{\boldsymbol{C}}\hat{\Psi}_\mathrm{aniso}(\boldsymbol{C}; \boldsymbol{M}) \quad \text{with} \quad p = U'(1) = 0\,. \tag{65}$$

Noting $\overline{\boldsymbol{S}} = 2\,\partial_{\boldsymbol{C}}\hat{\Psi}_\mathrm{iso}(\boldsymbol{C})$ we obtain the same stress governed by an incompressible material when the Lagrange multiplier $\tilde{p}$ in (15) takes the form

$$\tilde{p} = -\frac{2}{3}\mathrm{tr}_{\boldsymbol{C}}[\partial_{\boldsymbol{C}}\hat{\Psi}_\mathrm{iso}(\boldsymbol{C})] = -\frac{2}{3}\,\partial_{\boldsymbol{C}}\hat{\Psi}_\mathrm{iso}(\boldsymbol{C}) : \boldsymbol{C}\,. \tag{66}$$

It is governed only by the isotropic stored-energy function and for a neo-Hookean ground substance under simple shear we get

$$\tilde{p} = -\frac{1}{3}\mu(3+\gamma^2)\,. \tag{67}$$

[9] Note carefully that force measurements were made using a strain-controlled rheometer performing a torsion test. The translation of these *global (structural)* results to the *local* stress state of simple shear may not be obvious, especially when the material possesses a complex anisotropic microstructure. Again, we refer to the discussion in Section 4.

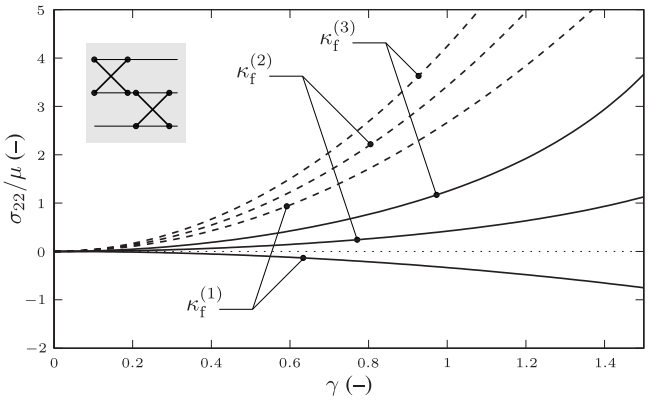

Fig. 5. Simple shear (horizontal alignment of the mean fibers $\phi = 90°$): lateral normal stress for different fiber dispersion parameters $\kappa_f^{(1)} = 0$ (ideal fiber alignment), $\kappa_f^{(2)} = 0.35$ and $\kappa_f^{(3)} = 0.5$ (uniform fiber distribution). The solid curves indicate the behavior without cross-links and the dashed curves with cross-links. In the latter case, the dimensionless parameters $\bar{\nu} = \nu/\mu = 3$ and $\bar{c} = c/\mu = 2$ are chosen. The other material parameters are $\bar{k}_1 = k_1/\mu = 2$ and $k_2 = 0.3$.

For our analysis we first neglect the fiber dispersion $\kappa_f = 0$. Then the fibers do not contribute, but the cross-links contribute via the non-negative term $A^+ = \nu\gamma^2 \geq 0$. The term B^+, representing the interaction between fiber and the cross-link, disappears. We find that the lateral normal stress σ_{22} has a *positive* sign if and only if the cross-link stiffness is $\nu > \mu/3$.

On the other hand, for dispersed fibers $\kappa_f \neq 0$ the stored energy related to the fiber stretch and the term $B^+ = c\kappa_f\gamma^2$ are active and the sign of σ_{22} can switch from negative to positive with increasing amount of shear γ, i.e. the sign change occurs at

$$\gamma = \frac{1}{k_2^{1/4}\sqrt{\kappa_f}}\left[\ln\left(-\frac{c\kappa_f^2 - \mu/3 + \nu}{2k_1\kappa_f^2}\right)\right]^{1/4} \qquad \text{for } \nu < \frac{\mu}{3} - \kappa_f^2(c + 2k_1)\,. \tag{70}$$

If the cross-links are stiff enough $\nu \geq \mu/3 - \kappa_f^2(c + 2k_1)$ the lateral normal stress remains positive during simple shear deformation. From the last expression we see that the fiber dispersion lowers the necessary cross-link stiffness required to obtain a lateral tensile normal stress σ_{22}. Taking a look at the sensitivities

$$\frac{\partial\sigma_{22}}{\partial\nu} = \gamma^2 \geq 0 \quad \text{and} \quad \frac{\partial\sigma_{22}}{\partial c} = \kappa_f^2\gamma^2 \geq 0\,, \tag{71}$$

we see that the dispersion does not affect the growth of the lateral normal stress with respect to an increasing cross-link stiffness, but determines the growth with respect to the cross-link-fiber interaction parameter. Without cross-links $\nu = c = 0$, the lateral normal stress is positive for all $\gamma > 0$ if and only if $\kappa_f \geq \sqrt{\mu/(6k_1)}$ for the fiber dispersion parameter. Recalling the admissible range $\kappa_f \in [\,0, 1/2\,]$ we see from the last expression that σ_{22} cannot be tensile throughout the simple shear deformation if the shear modulus is too high $\mu > 3/2\,k_1$.

In Fig. 5 the lateral normal stress response is plotted for the dimensionless parameters $\bar{k}_1 = k_1/\mu = 2$ and $k_2 = 0.3$. Looking at the solid curves, which do not indicate cross-links, we see a transition from compressive to tensile stress as the value of the fiber dispersion parameter κ_f increases. From the dashed curves we observe that the presence of cross-links strongly supports the tendency of the specimen to contract laterally, as indicated in the sensitivities (71). In this example, the dimensionless cross-link stiffness and the cross-link-fiber interaction parameter are set to $\bar{\nu} = \nu/\mu = 3$ and $\bar{c} = c/\mu = 2$.

Next we want to point out the difference in the results for the lateral normal stress when the volumetric–isochoric split is also applied on the anisotropic part of the stored-energy function. In this case, neglecting the fiber dispersion $\kappa_f = 0$ for simplicity, we obtain for the lateral normal stress after some calculations not given here

$$\widetilde{\sigma}_{22} = -\frac{\gamma^2}{3}[\,\mu + (\gamma^2 - 1)\nu + 4\kappa_c^2(c + 4\nu)\,]\,, \tag{72}$$

where we put the tilde sign to distinguish this result from (69), which takes the simple form

$$\sigma_{22} = -\frac{\gamma^2}{3}(\mu - 3\nu)\,. \tag{73}$$

Comparing the expressions (72) and (73) we find fundamental qualitative differences. First, $\widetilde{\sigma}_{22}$ is affected by fiber-independent cross-link dispersion via the parameter κ_c, while σ_{22} is not (as mentioned above). Second, recalling the admissible range $\kappa_c \in [\,1/\pi, 1/2\,]$ for the fiber-independent cross-link dispersion parameter, we find that $\widetilde{\sigma}_{22}$ is always compressive and decreases with increasing cross-link stiffness ν. This behavior is non-intuitive, as can be understood by considering two single cross-links represented by the directors $[\,\boldsymbol{L}^{\pm}\,] = [\,\pm\cos\beta,\ \sin\beta,\ 0\,]^T$ with $\beta = 45°$: the stretches of the cross-links under simple shear become $\lambda^2(\boldsymbol{L}^{\pm}) = \gamma^2/2 \pm \gamma + 1$ and we observe that the cross-link connected to $\boldsymbol{L}^+$ is under tension and the cross-link connected to $\boldsymbol{L}^-$ is under tension/compression for $\gamma \gtrless 2$. So if we remove the kinematic constraint at the top or bottom (perhaps at high enough amount of shear), we expect the

body to contract in the lateral direction. This circumstance raises another doubt in the volumetric–isochoric split applied on the anisotropic part of the stored-energy function. Fig. 6 depicts the lateral normal stress response for both the 'incomplete' and the 'complete' volumetric–isochoric split for different values of the cross-link stiffness ν.

Finally, if we neglect the fiber dispersion $\kappa_\mathrm{f} = 0$ and the cross-links $\nu = 0$ in (69), we recover the *standard isotropic* case, so worth some remarks;

Remark (*Isotropy*)**.** For the considered *nearly incompressible* ansatz, the neo-Hookean model results in a negative lateral normal stress $\sigma_{22} = -\mu/3\,\gamma^2$ which means that the top and bottom faces have a tendency to spread apart. In the case of an *incompressible* material, the unknown Lagrange multiplier $\widetilde{p} \in \mathbb{R}$ in (15) is in the literature often determined for the simple shear mode by either

(i) the condition of plane stress[10] $\sigma_{33} = 0$, or
(ii) the condition of vanishing normal traction on the inclined faces $\sigma_{22} - [\gamma/(1+\gamma^2)]\,\sigma_{12} = 0$.

Depending on which of these kinetic conditions are set, and assuming a stored-energy function $\widetilde{\Psi}(I_1)$ that depends only on the first principal invariant I_1, we obtain either (i) a vanishing lateral normal stress, or, if the inequality $\partial_{I_1}\widetilde{\Psi} > 0$ holds, (ii) a positive lateral normal stress. Note that for the kinetic condition (i) of the plane stress, a non-zero normal stress σ_{22} can only be obtained by considering the second principal invariant I_2 in the stored-energy function $\widetilde{\Psi}(I_1, I_2)$, see Horgan and Murphy (2011, 2017) and Destrade et al. (2015).[11] More specifically, these references state that for condition (i) the lateral normal stress is compressive/tensile if $\partial_{I_2}\widetilde{\Psi} \gtrless 0$. Usually this is controlled by the sign of a material parameter.

To get rid of the ambiguity regarding the compressive or tensile nature of the lateral stress σ_{22} resulting from the choice of the kinetic condition (i) or (ii) in the case of incompressibility, a nearly incompressible framework as in Horgan and Murphy (2010) is imposed. As mentioned in Footnote , for an isochoric deformation the stress obtained by the nearly incompressible ansatz can also be generated by an incompressible framework if the Lagrange multiplier $\widetilde{p}$ is set to (67), which does not involve any kinetic assumption.

3.2.2. Vertical mean fiber direction

Next we consider the case of vertical mean fibers $\phi = 0°$ and the expression (68) simplifies to

$$\sigma_{22} = -\frac{\mu}{3}\gamma^2 + 2(1-\kappa_\mathrm{f})\widetilde{\Psi}_\mathrm{f}'(I_4) + A^+ + (1-\kappa_\mathrm{f})B^+ \,. \tag{74}$$

Here, too, we see immediately that the lateral normal stress is independent of the parameter κ_c. Comparing (74) with (69) shows a difference in the factor multiplied with the second and fourth terms.

Neglecting the fiber dispersion $\kappa_\mathrm{f} = 0$ we see that both the fibers and the cross-links contribute to σ_{22}. In contrast to the case of horizontal mean fiber directions, the cross-links also affect the lateral normal stress via the term $B^+ = c\gamma^2$, i.e. the cross-link-fiber interaction parameter c plays a role. With increasing amount of shear γ, the lateral normal stress can switch from compressive to tension, i.e. the transition occurs at

$$\gamma = \frac{1}{k_2^{1/4}}\left[\ln\left(-\frac{c-\mu/3+\nu}{2k_1}\right)\right]^{1/4} \qquad \text{for } \nu < \frac{\mu}{3} - (c+2k_1)\,. \tag{75}$$

With sufficiently stiff cross-links ($\nu \geq \mu/3 - (c+2k_1)$) the lateral normal stress σ_{22} remains positive throughout simple shear deformation. We observe that less stiff cross-links are required to generate a lateral tensile normal stress attributable to the stretched fibers compared to horizontally aligned fibers.

For dispersed fibers $\kappa_\mathrm{f} \neq 0$ the sign of σ_{22} can switch from negative to positive again with increasing amount of shear γ, i.e. the sign changes at

$$\gamma = \frac{1}{k_2^{1/4}\sqrt{1-\kappa_\mathrm{f}}}\left[\ln\left(-\frac{c(1-\kappa_\mathrm{f})^2-\mu/3+\nu}{2k_1(1-\kappa_\mathrm{f})^2}\right)\right]^{1/4} \qquad \text{for } \nu < \frac{\mu}{3} - (1-\kappa_\mathrm{f})^2(c+2k_1)\,. \tag{76}$$

For sufficiently stiff cross-links ($\nu \geq \mu/3-(1-\kappa_\mathrm{f})^2(c+2k_1)$) the lateral normal stress throughout simple shear deformation is tensile. We observe that, in contrast to a horizontal mean fiber direction, fiber dispersion increases the cross-link stiffness required to obtain a lateral tensile normal stress. Taking a look at the sensitivities

$$\frac{\partial\sigma_{22}}{\partial\nu} = \gamma^2 \geq 0 \quad \text{and} \quad \frac{\partial\sigma_{22}}{\partial c} = (1-\kappa_\mathrm{f})\gamma^2 \geq 0\,, \tag{77}$$

we find again that the dispersion does not affect the growth of the lateral normal stress with respect to an increasing cross-link stiffness, but determines the growth with respect to the cross-link-fiber interaction parameter. If there are no cross-links ($\nu = c = 0$),

[10] Recalling that we are considering the scenario of plane strain ($\lambda_3 = 1$), the imposition of the condition $\sigma_{33} = 0$ may not be permissible since the out-of-plane direction becomes overconstrained. A model that *constitutively* determines $\sigma_{33} = 0$ for $\lambda_3 = 1$ may exist, but such an adjustment seems neither practical nor desirable. Nevertheless, for a comparison with the compressible ansatz, which does not require any additional kinetic assumption, we also consider the plane stress state for the incompressible setting in the following. It should also be noted that for *inhomogeneous* problems the Lagrange multiplier *field* $\widetilde{p}$ is determined via the mechanical equilibrium and no (possibly 'mixed up') additional kinetic condition is required, see also Section 4.

[11] In the case of simple shear, the second principal invariant coincides with the first, $I_1 = I_2 = 3 + \gamma^2$.

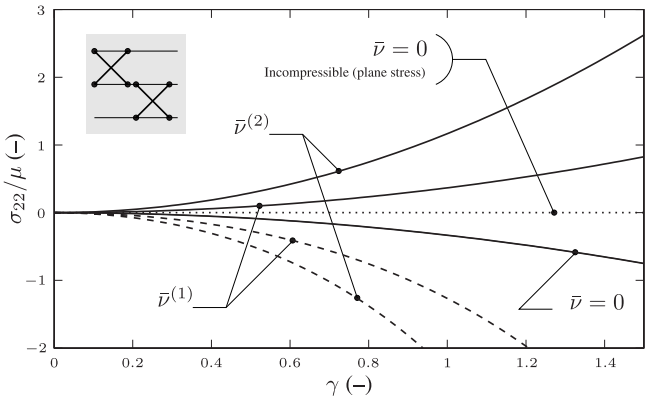

Fig. 6. Simple shear (horizontal alignment of mean fibers $\phi = 90°$) – 'complete' versus 'incomplete' volumetric–isochoric split: fiber dispersion is ignored $\kappa_f = 0$. The solid curves indicate the lateral normal stress obtained by applying the 'incomplete' volumetric–isochoric split (12) for increasing values of the dimensionless cross-link stiffness, i.e. $\bar{\nu}^{(1)} = 0.7$ and $\bar{\nu}^{(2)} = 1.5$. The dashed curves show the behavior for the 'complete' split ($\bar{c} = c/\mu = 0$ and $\kappa_c = 1/2$), i.e. the unimodular part $\overline{C}$ of the right Cauchy–Green tensor is used to formulate the anisotropic part of the stored-energy function. For $\bar{\nu} = 0$ both formulations coincide. If one considers an incompressible material and determines the Lagrange multiplier $\tilde{p}$ by the condition of plane stress, then the lateral normal stress vanishes.

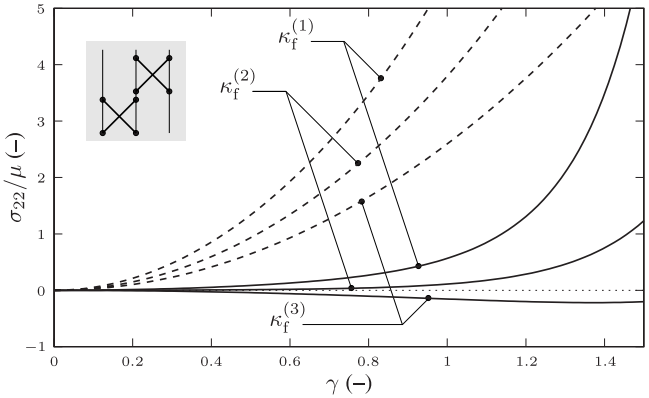

Fig. 7. Simple shear (vertical alignment of the mean fibers $\phi = 0°$): lateral normal stress for different fiber dispersion parameters $\kappa_f^{(1)} = 0$ (ideal fiber alignment), $\kappa_f^{(2)} = 0.25$ and $\kappa_f^{(3)} = 0.5$ (uniform fiber distribution). The solid curves show the behavior without cross-links and the dashed curves with cross-links. In the latter case, the dimensionless parameters $\bar{\nu} = \nu/\mu = 2$ and $\bar{c} = c/\mu = 3$ are chosen. The other material parameters are $\bar{k}_1 = k_1/\mu = 1/3$ and $k_2 = 0.3$.

the lateral normal stress σ_{22} is positive for all $\gamma > 0$ if and only if $\kappa_f \leq 1 - \sqrt{\mu/(6k_1)}$. Recalling the admissible range $\kappa_f \in [\,0, 1/2\,]$ we observe from the last expression that σ_{22} cannot be tensile throughout simple shear deformation, if the shear modulus is too high $\mu > 6k_1$.

Fig. 7 shows the lateral normal stress response for the dimensionless parameters $\bar{k}_1 = k_1/\mu = 1/3$ and $k_2 = 0.3$. Looking at the solid curves that indicate no cross-links, we see a transition from positive to negative normal stress for an increasing fiber dispersion parameter κ_f. Note that for $\kappa_f = 0.5$ (isotropy), the stress σ_{22} is compressive for $0 < \gamma < 1.744$ and tensile for $\gamma > 1.744$, which can be found by evaluating (76). From the dashed curves it can be seen that cross-links favor the change from compressive to tensile lateral stress, as also shown by the sensitivities (77). In this example we have specified the dimensionless cross-link stiffness and the cross-link-fiber interaction parameter as $\bar{\nu} = \nu/\mu = 2$ and $\bar{c} = c/\mu = 3$. Again, we want to point out the opposite influence of the fiber dispersion on the lateral normal stress compared to the case of horizontal mean fiber directions discussed in Section 3.2.1, i.e. the more the fibers are dispersed, the less/more the body wants to expand in the lateral direction in case of vertical/horizontal mean fiber directions.

3.2.3. *Inclined mean fiber direction*

Finally, we consider an inclined mean fiber direction and want to investigate the influence of the fiber-independent cross-link dispersion governed by the parameter $\kappa_c \in [\,1/\pi, 1/2\,]$. For the sake of simplicity, we neglect the fiber dispersion $\kappa_f = 0$. Then the expression (68) for the lateral normal stress simplifies to

$$\sigma_{22} = -\frac{\mu}{3}\gamma^2 + A^+ + [\,2\widetilde{\Psi}_f'(I_4) + B^+\,]\cos^2\phi + \kappa_c(2A^- + B^-)\sin 2\phi\,. \tag{78}$$

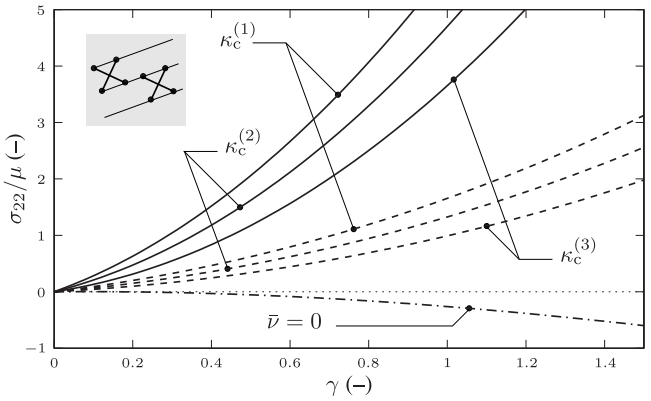

Fig. 8. Simple shear (inclined alignment of the fibers $\phi = 70°$): lateral normal stress for different cross-link dispersion parameters $\kappa_c^{(1)} = 1/2$ (ideal cross-link alignment), $\kappa_c^{(2)} = 0.42$ and $\kappa_c^{(3)} = 1/\pi$ (uniform distribution of cross-links). The solid curves correspond to cross-links with dimensionless stiffness $\bar{\nu} = \nu/\mu = 2.5$ and the dashed curves to cross-links with dimensionless stiffness $\bar{\nu} = \nu/\mu = 0.8$. In both cases, the dimensionless cross-link-fiber interaction parameter $\bar{c} = c/\mu$ is set to zero. The dash-dotted curve shows the behavior without cross-links. The other material parameters are chosen as $\bar{k}_1 = k_1/\mu = 1/3$ and $k_2 = 0.3$.

From there, we compute the sensitivity

$$\frac{\partial \sigma_{22}}{\partial \kappa_c} = 2\kappa_c \gamma (4\nu + c)(\gamma \sin 2\phi - 2\cos 2\phi) \sin 2\phi \,, \tag{79}$$

which is non-negative for all $\gamma \geq 0$ if and only if $\phi = 0°$ or $\phi \geq 45°$. Therefore, for this range of fiber angles, the lateral normal stress σ_{22} increases with increasing cross-link dispersion parameter κ_c, i.e. the more the dispersed cross-links are, the less the (global) stiffness becomes, see Fig. 8. Here, different cross-link stiffnesses $\bar{\nu} = \nu/\mu \in \{0, 0.8, 2.5\}$ are chosen and the interaction between the fiber and the cross-link is not taken into account ($\bar{c} = c/\mu = 0$). The dimensionless fiber-related material parameters are set to $\bar{k}_1 = k_1/\mu = 0.3$ and $k_2 = 0.3$. Again, we observe that the presence of (sufficiently stiff) cross-links leads to a tendency of approaching top and bottom faces. With that in mind, we take a look at the sensitivity, i.e.

$$\frac{\partial \sigma_{22}}{\partial \nu} = \gamma^2 + 4\kappa_c \nu (\gamma \sin 2\phi - 2\cos 2\phi) \sin 2\phi \,, \tag{80}$$

which is non-negative for all $\gamma \geq 0$ if and only if $\phi = 0°$ or $\phi \geq 45°$. Hence, for acute fiber angles ϕ, an increase in cross-link stiffness can lead to a stress decrease, at least locally, i.e. to an increase in compressive stress.

4. The Poynting effect under pure torsion

Now we want to consider the *nonhomogeneous* problem of pure torsion. We take a long circular hollow cylinder with an initial inner radius a_0 and an initial outer radius b_0 subjected to a twisting moment at its ends. We choose cylindrical coordinates (R, Θ, Z) and (r, θ, z) with associated unit base vectors $(\boldsymbol{E}_R, \boldsymbol{E}_\Theta, \boldsymbol{E}_Z)$ and $(\boldsymbol{e}_r, \boldsymbol{e}_\theta, \boldsymbol{e}_z)$ built at points of the reference and current configuration, respectively. The deformation map takes on the form

$$\varphi_r = R \,, \quad \varphi_\theta = \Theta + \vartheta Z \,, \quad \varphi_z = Z \,, \tag{81}$$

where ϑ denotes the twist per unit length. The right Cauchy–Green tensor becomes

$$\boldsymbol{C} = \boldsymbol{1} + R^2 \vartheta^2 \boldsymbol{E}_Z \otimes \boldsymbol{E}_Z + 2R\vartheta \, \mathrm{sym}[\boldsymbol{E}_\Theta \otimes \boldsymbol{E}_Z] \,. \tag{82}$$

Comparing the deformation tensors $(84)_2$ defined below and $(63)_2$ we observe that the inhomogeneous deformation of pure torsion can *locally* be identified with the deformation mode of simple shear (formally replace $R\vartheta$ by the amount of shear γ). For the sake of simplicity, we only consider one fiber family in the following, which is symmetrically dispersed in the $(\boldsymbol{E}_\Theta, \boldsymbol{E}_Z)$ planes. It is assumed that the dispersion of the cross-links is only induced by the fiber dispersion and the dispersion parameters $\widetilde{\kappa}$ and κ_c are represented by (28). The material is assumed to be incompressible and the invariants are built by the right Cauchy–Green tensor (82). We are particularly interested in the resultant normal force N, which acts on one end of the cylindrical specimen and is necessary to maintain the deformation. Note that this Poynting effect under torsion has to be investigated separately from that under simple shear, since the axial normal stress σ_{zz} due to torsion can spatially switch its sign without changing the compressive or tensile nature of the resultant normal force, see also Horgan and Murphy (2017). With that in mind, recall that we are observing for the simple shear configurations discussed in Sections 3.2.1 and 3.2.2 a switch in the sign of the lateral normal stress at certain deformation levels.

We consider the push-forward of the second Piola–Kirchhoff stress tensor (15), which gives the Cauchy stress tensor

$$\begin{aligned}\boldsymbol{\sigma} = \widetilde{p}\boldsymbol{1} \;&+\; \mu\boldsymbol{b} + \{\, 2\kappa_{\mathrm{f}}\widetilde{\Psi}'_{\mathrm{f}}(I_4) + \kappa_{\mathrm{f}}B^{+} + A^{+} + [\,\kappa_{\mathrm{f}}B^{+} - (1-2\kappa_{\mathrm{f}})A^{+}\,]\cos 2\beta\,\}\overset{(2)}{\boldsymbol{b}} \\ &+ (1-2\kappa_{\mathrm{f}})[\,2\widetilde{\Psi}'_{\mathrm{f}}(I_4) + B^{+} + (B^{+}+2A^{+})\cos 2\beta\,]\,\boldsymbol{m}\otimes\boldsymbol{m} \\ &+ [\,(1-2\kappa_{\mathrm{f}})(2A^{-}+B^{-})\sin 2\beta\,]\;\mathrm{sym}[\boldsymbol{m}\otimes\boldsymbol{m}_{\mathrm{n}}]\end{aligned} \tag{83}$$

in terms of the two- and three-dimensional left Cauchy–Green tensor

$$\overset{(2)}{\boldsymbol{b}} = \overset{(2)}{\boldsymbol{1}} + R^2\vartheta^2\boldsymbol{E}_{\Theta}\otimes\boldsymbol{E}_{\Theta} + 2R\vartheta\;\mathrm{sym}[\boldsymbol{E}_{\Theta}\otimes\boldsymbol{E}_{Z}] \quad\text{and}\quad \boldsymbol{b} = \overset{(2)}{\boldsymbol{b}} + \boldsymbol{E}_{R}\otimes\boldsymbol{E}_{R}\,, \tag{84}$$

and the push-forwards of the structural director and its normal

$$\boldsymbol{m} = \boldsymbol{M} + R\vartheta\cos\phi\,\boldsymbol{E}_{\Theta} \quad\text{and}\quad \boldsymbol{m}_{\mathrm{n}} = \boldsymbol{M}_{\mathrm{n}} + R\vartheta\sin\phi\,\boldsymbol{E}_{\Theta}\,. \tag{85}$$

The expressions $A^{\pm}$ and $B^{\pm}$ are given in (43) and depend on the invariants $I^{\pm}$ and $I_8^{\star\pm}$ specified below. The shear stresses $\sigma_{r\theta}$ and σ_{rz} in (83) vanish. All non-zero components of the Cauchy stress tensor (83) depend only on the radial coordinate R, and the mechanical equilibrium condition (without volume loads and inertia) reduces to

$$R\,\frac{\mathrm{d}}{\mathrm{d}R}\sigma_{rr} - (\sigma_{\theta\theta}-\sigma_{rr}) = 0\,, \qquad \frac{\mathrm{d}}{\mathrm{d}R}(R^2\sigma_{r\theta}) = 0\,, \qquad \frac{\mathrm{d}}{\mathrm{d}R}(R\,\sigma_{rz}) = 0 \tag{86}$$

for $R\in(a_0,b_0)$ together with the homogeneous boundary conditions $\sigma_{rr}(R=a_0)=0$ and $\sigma_{rr}(R=b_0)=0$. The conditions $(86)_{2-3}$ are trivially fulfilled, whereas $(86)_1$ serves as the equation for determining the Lagrange multiplier $\widetilde{p}$, which is a function of R. The resultant normal force N, which acts on one end of the specimen, is simply calculated from

$$N = 2\pi\int_{a_0}^{b_0}\sigma_{zz}R\,\mathrm{d}R\,. \tag{87}$$

Subtracting the zero term

$$\pi R^2[\,\sigma_{rr}(b_0)-\sigma_{rr}(a_0)\,] = \pi\int_{a_0}^{b_0}\frac{\mathrm{d}}{\mathrm{d}R}(R^2\sigma_{rr})\,\mathrm{d}R \tag{88}$$

from (87), by taking into account the equilibrium equation $(86)_1$, we get an alternative representation for the resultant normal force as

$$N = \pi\int_{a_0}^{b_0}[\,2\sigma_{zz}-(\sigma_{rr}+\sigma_{\theta\theta})\,]\,R\,\mathrm{d}R\,. \tag{89}$$

Note carefully that the Lagrange multiplier $\widetilde{p}$ does *not arise* in the latter integrand. Hence, the expression (89) is subsequently used to calculate the normal force N. We introduce the dimensionless quantity $\bar{N} = N/(\pi\mu a_0^2)$ and examine its variation with respect to $\bar{\vartheta} = \vartheta\,a_0$. The direction $\boldsymbol{M}$ of the mean fibers is now set to two cases.

4.1. Axial mean fiber direction

First we consider mean fibers that are parallel to the axis of the cylindrical specimen, i.e. $\boldsymbol{M} = \boldsymbol{E}_Z$. The invariants take the specific forms

$$I_1 = 3 + R^2\vartheta^2\,, \tag{90}$$

$$I_4 = \kappa_{\mathrm{f}} + (1-\kappa_{\mathrm{f}})(1+R^2\vartheta^2)\,, \tag{91}$$

$$I^{\pm} = \frac{1}{2}[\,2 + R^2\vartheta^2 + R\vartheta(1-2\kappa_{\mathrm{f}})(R\vartheta\cos 2\beta \mp 2\sin 2\beta)\,]\,, \tag{92}$$

$$I_8^{\star\pm} = I_4\cos^2\beta \mp R\vartheta(1-2\kappa_{\mathrm{f}})\sin\beta\cos\beta \tag{93}$$

in terms of the angle β describing the orientation of the cross-links relative to a parallel pair of dispersed fibers. From (83) we can extract the Cauchy normal stresses in the radial, azimutal and axial directions

$$\sigma_{rr} = \widetilde{p} + \mu\,, \tag{94}$$

$$\begin{aligned}\sigma_{\theta\theta} = \widetilde{p} + (1+R^2\vartheta^2)\{\,&\mu + 2\kappa_{\mathrm{f}}\widetilde{\Psi}'_{\mathrm{f}}(I_4) + \kappa_{\mathrm{f}}B^{+} + A^{+} + [\kappa_{\mathrm{f}}B^{+} - (1-2\kappa_{\mathrm{f}})A^{+}]\cos 2\beta\,\} \\ &+ R^2\vartheta^2(1-2\kappa_{\mathrm{f}})\,[\,2\widetilde{\Psi}'_{\mathrm{f}}(I_4) + B^{+} + (B^{+}+2A^{+})\cos 2\beta\,] \\ &- R\vartheta(1-2\kappa_{\mathrm{f}})(2A^{-}+B^{-})\sin 2\beta\,,\end{aligned} \tag{95}$$

$$\sigma_{zz} = \widetilde{p} + \mu + (1-\kappa_{\mathrm{f}})\,[\,2\widetilde{\Psi}'_{\mathrm{f}}(I_4) + B^{+}\,] + A^{+} + [\kappa_{\mathrm{f}}B^{+} + (1-2\kappa_{\mathrm{f}})(A^{+}+B^{+})]\cos 2\beta\,. \tag{96}$$

The expression for the dimensionless normal force $\bar{N}$ obtained from (89) is quite long and is not explicitly given here. However, we note that it contains the imaginary error function $\mathrm{erfi}[m(1-\kappa_{\mathrm{f}})\bar{\vartheta}^2]$, $m>0$, defined as $\mathrm{erfi}(x) = -\mathrm{i}\,\mathrm{erf}(\mathrm{i}x)$. In the undeformed state $\bar{\vartheta}=0$ we have to be aware of the limit property $\lim_{x\to 0}\mathrm{erfi}(x)/x = 2/\sqrt{\pi}$ to get $\bar{N}=0$.

We start by setting the relative cross-link orientation to $\beta = 90°$ and find $I_8^{\star\pm}=0$, i.e. the mechanical response is independent of the cross-link-fiber interaction parameter c. The relevant dimensionless material parameters are specified as $\bar{k}_1 = k_1/\mu = 1$, $k_2 = 0.3$

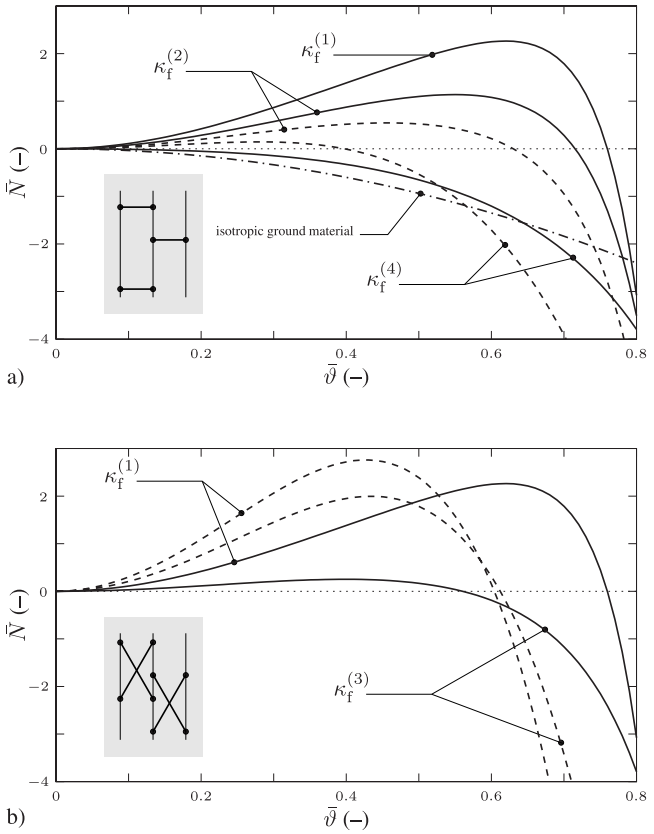

Fig. 9. Pure torsion ($\phi = 0°$): normal force response for cross-link orientations (a) $\beta = 90°$ and (b) $\beta = 30°$ for different values of the fiber dispersion parameter $\kappa_f^{(1)} = 0$ (ideal fiber alignment), $\kappa_f^{(2)} = 0.1$, $\kappa_f^{(3)} = 0.25$ and $\kappa_f^{(4)} = 0.45$. The ratio between the outer and the inner radius of the cylindrical specimen is chosen to be $b_0/a_0 = 2$. The solid curves show the behavior without cross-links and the dashed curves with cross-links, where we set $\bar{\nu} = \nu/\mu = 2$ in (a) and additionally $\bar{c} = c/\mu = 1$ in (b). The other material parameters are $\bar{k}_1 = k_1/\mu = 1$ and $k_2 = 0.3$. The dash-dotted curve in (a) shows the mechanical response for the isotropic ground material of the neo-Hookean type.

and $\bar{\nu} = 2$, as well as the ratio between the outer and inner radius of the cylindrical specimen is set to $b_0/a_0 = 2$. Fig. 9(a) shows the dimensionless normal force $\bar{N}$ over $\bar{\vartheta}$ for different values of the fiber dispersion parameter κ_f. The solid curves indicate the behavior without cross-links and the dashed ones with cross-links. First, we observe that the presence of perfectly aligned fibers (the cross-links do not play a role for $\kappa_f = 0$) leads to a tensile normal force, at least for moderate deformations, while a specimen that just consists of the neo-Hookean ground material exhibits a compressive normal force as shown by the dash-dotted curve.

Remark. Note that in case of simple shear, the lateral normal stress vanishes for the additional condition of plane stress imposed on an incompressible neo-Hookean material. In contrast, for the (slightly) compressible ansatz depicted in Fig. 6 (or the incompressible ansatz using a stored-energy function with $\partial_{I_2}\widetilde{\Psi} > 0$ under the additional condition of plane stress) a negative lateral normal stress is observed, i.e. the positive Poynting effect under torsion can be transferred to the deformation mode of simple shear.

As the fibers get dispersed, the normal force decreases until it changes its sign. In a certain range of κ_f this tendency is 'accelerated' by the presence of cross-links – at least in the region of moderate deformations – as can be seen for $\kappa_f = 0.1$ in Fig. 9(a), i.e. the solid curve lies above the dashed one. However, when the fibers are sufficiently dispersed, this trend is reversed by the presence of cross-links, as can be seen for $\kappa_f = 0.45$ in the domain of moderate deformations, i.e. part of the solid curve lies below the dashed one. This is because with a high fiber dispersion, more cross-links are closely oriented in the direction $\boldsymbol{M} = \boldsymbol{E}_Z$.

Next, we consider the case $\beta = 30°$, which is depicted in Fig. 9(b). We choose the same dimensionless material parameters $\bar{k}_1$, k_2 and $\bar{\nu}$ as before and we additionally set $\bar{c} = c/\mu = 1$. Again, we take $b_0/a_0 = 2$. We observe that fiber dispersion leads to a decrease in the tensile normal force for the setup with and without cross-links. In contrast to the previous cross-link configuration with $\beta = 90°$, the cross-links 'slowdown' the tendency to switch the sign of the normal force in the moderate deformation range for all possible fiber dispersion parameters, i.e. parts of the solid curves lie below the dashed ones. This is because at the cross-link orientation $\beta = 30°$ the stiffest configuration can be expected in the range of moderate deformations when the fibers are perfectly aligned along $\boldsymbol{M} = \boldsymbol{E}_Z$.

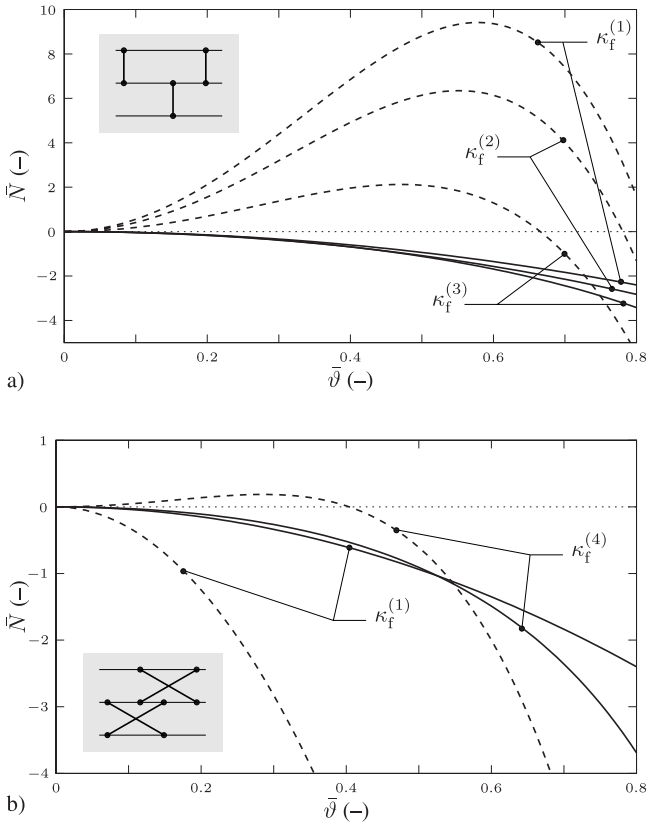

Fig. 10. Pure torsion ($\phi = 90°$): normal force response for cross-link orientations (a) $\beta = 90°$ and (b) $\beta = 30°$ for varying values of the fiber dispersion parameter $\kappa_f^{(1)} = 0$ (ideal fiber alignment), $\kappa_f^{(2)} = 0.1$, $\kappa_f^{(3)} = 0.3$ and $\kappa_f^{(4)} = 0.45$. The geometry of the cylindrical specimen is specified by the ratio $b_0/a_0 = 2$. The solid curves indicate the behavior without cross-links and the dashed curves with cross-links, where in (a) we set $\bar{\nu} = \nu/\mu = 2$ and additionally $\bar{c} = c/\mu = 1$ in (b). The other material parameters are $\bar{k}_1 = k_1/\mu = 1$ and $k_2 = 0.3$.

4.2. Azimutal mean fiber direction

Second, we take the mean fibers to be oriented along the azimutal direction, i.e. $\boldsymbol{M} = \boldsymbol{E}_\Theta$. The invariants specify to

$$I_4 = (1-\kappa_f) + \kappa_f(1 + R^2\vartheta^2)\,, \tag{97}$$

$$I^{\pm} = 1 + \kappa_f R^2\vartheta^2 \pm R\vartheta(1-2\kappa_f)(\sin 2\beta \pm R\vartheta \sin^2\beta)\,, \tag{98}$$

$$I_8^{\star\pm} = I_4 \cos^2\beta \pm R\vartheta(1-2\kappa_f)\sin\beta\cos\beta\,, \tag{99}$$

and I_1 is of course identical to (90). The Cauchy normal stresses in the radial, azimutal and axial directions are

$$\sigma_{rr} = \widetilde{p} + \mu\,, \tag{100}$$

$$\begin{aligned}\sigma_{\theta\theta} = \widetilde{p} + (1+R^2\vartheta^2)\{\,&\mu + 2\kappa_f\widetilde{\Psi}_f'(I_4) + \kappa_f B^+ + A^+ + [\kappa_f B^+ - (1-2\kappa_f)A^+]\cos 2\beta\,\} \\ &+ (1-2\kappa_f)\,[\,2\widetilde{\Psi}_f'(I_4) + B^+ + (B^+ + 2A^+)\cos 2\beta\,] \\ &+ R\vartheta(1-2\kappa_f)(2A^- + B^-)\sin 2\beta\,,\end{aligned} \tag{101}$$

$$\sigma_{zz} = \widetilde{p} + \mu + 2\kappa_f\widetilde{\Psi}_f'(I_4) + \kappa_f B^+ + A^+ + [\,\kappa_f B^+ - (1-2\kappa_f)A^+\,]\cos 2\beta\,. \tag{102}$$

From (89) we get the dimensionless normal force $\bar{N}$, whose expression is quite long and is not explicitly given here. However, we mention that it contains the term $\mathrm{erfi}[m\kappa_f\bar{\vartheta}^2]$, $m > 0$, and again we have to be aware of the limit property of the imaginary error function for $\kappa_f \to 0$ (perfect fiber alignment) or $\bar{\vartheta} \to 0$.

We fix the relative cross-link orientation to $\beta = 90°$ and find $I_8^{\star\pm} = 0$ as before, i.e. the mechanical response does not depend on the cross-link-fiber interaction parameter c. As in Section 4.1 the other material parameters are set to $\bar{k}_1 = k_1/\mu = 1$, $k_2 = 0.3$ and $\bar{\nu} = \nu/\mu = 2$, and we set $b_0/a_0 = 2$. Fig. 10(a) shows the dimensionless normal force $\bar{N}$ versus $\bar{\vartheta}$ for varying values of the fiber dispersion parameter κ_f. We observe a pronounced difference between the normal forces for cross-linked and non cross-linked cylindrical specimens under torsion. In the presence of cross-links, increasing fiber dispersion decreases the overall stiffness in

the moderate deformation range. Again, this is not surprising since we can expect that cross-links oriented along the cylindrical specimen's axis $\boldsymbol{E}_Z$ provide the stiffest configuration. Without cross-links we observe a compressive normal force. If the fiber dispersion is sufficiently high, the fibers are oriented more closely in the direction $\boldsymbol{E}_Z$, which leads to a tendency to change the sign of the normal force in the moderate deformation range, as can be observed better from the solid curves in Fig. 10(b).

Finally, we consider a cross-link orientation given by the angle $\beta = 30°$. This scenario is depicted in Fig. 10(b). We choose the same dimensionless material parameters $\bar{k}_1$, k_2 and $\bar{\nu}$ as before and choose additionally $\bar{c} = c/\mu = 1$. Again we set $b_0/a_0 = 2$. From the dashed curves it can be clearly seen that the presence of cross-links coupled with a sufficiently high fiber dispersion leads to a switch in the sign of the normal force for moderate deformations. In contrast, without cross-links, the normal force remains compressive.

5. Conclusion

In this study, we developed a plane strain continuum model that accounts for a statistical orientation distribution of fiber-connecting cross-links. It is essentially based on two geometric considerations, namely a cross-link dispersion induced by fiber dispersion and a fiber-independent dispersion of cross-links. Both mechanisms define the structure tensors that govern the invariants that enter the stored-energy function. The kinematics is based on a classical multiplicative split of the deformation gradient into volumetric and isochoric parts, which, however, was only applied to the isotropic part in order to obtain physically meaningful results. The proposed model has been examined in detail for the cases of homogeneous uniaxial extension and simple shear. We observe a stiffening of the tissue due to the presence of cross-links and a significant dependence of the stress response on the statistical orientation distribution of fibers and cross-links.

In the case of simple shear deformation, particular attention was paid to the normal stress generated perpendicular to the shear planes (Poynting effect). We used a compressible formulation to describe the isochoric deformation of simple shear. This was done to remove the sensitivity of the sign of the normal stress considered, which results from the additional constraint that needs be imposed to evaluate the Lagrange multiplier in the case of an incompressible material. We found that the cross-links play a major role in the deformation behavior of the specimen perpendicular to the shear direction, i.e. when the shear planes tend to move apart (negative normal stress) or tend to contract (positive normal stress). For example, in the case of a horizontal (mean) fiber direction, we found that sufficiently stiff cross-links switch the considered normal stress from compression to tension. Therefore, one may suspect that the tensile normal stress effects observed in simple shear experiments of biopolymers are (not only, but also) related to the presence of cross-links in the material.

Finally we considered pure torsion applied to a circular hollow cylinder. We studied the associated Poynting effect, i.e. the axial normal force that is necessary to maintain the deformation. We have again found that the cross-linked fibrous microstructure has a pronounced influence on the mechanical (tensile or compressive) response of the specimen.

Declaration of competing interest

The authors declare that they have no known competing financial interests or personal relationships that could have appeared to influence the work reported in this paper.

Acknowledgments

The authors' work was partly supported by the Lead Project on 'Mechanics, Modeling and Simulation of Aortic Dissection', granted by Graz University of Technology.

References

Advani, S.G., Tucker III, C.L., 1987. The use of tensors to describe and predict fiber orientation in short fiber composites. J. Rheol. 31 (8), 751–784.

Åström, J.A., Kumar, P.S., Vattulainen, I., Karttunen, M., 2008. Strain hardening, avalanches, and strain softening in dense cross-linked actin networks. Phys. Rev. E 77 (5), 051913.

Bailey, A.J., 2001. Molecular mechanisms of ageing in connective tissues. Mech. Ageing Dev. 122 (7), 735–755.

Barodka, V.M., Joshi, B.L., Berkowitz, D.E., Hogue Jr., C.W., Nyhan, D., 2011. Review article: Implications of vascular aging. Anesth. Analg. 112 (5), 1048–1060.

Boehler, J.P. (Ed.), 1987. Applications of Tensor Functions in Solid Mechanics. In: CISM Courses and Lectures no. 292, Springer-Verlag, Wien.

Buehler, M.J., 2008. Nanomechanics of collagen fibrils under varying cross-link densities: atomistic and continuum studies. J. Mech. Behav. Biomed. Mater. 1 (1), 59–67.

Chen, Y.-C., Chen, M., Gaffney, E.A., Brown, C.P., 2017. Effect of crosslinking in cartilage-like collagen microstructures. J. Mech. Behav. Biomed. Mater. 66, 138–143.

Conti, E., MacKintosh, F.C., 2009. Cross-linked networks of stiff filaments exhibit negative normal stress. Phys. Rev. Lett. 102 (8), 088102.

Depalle, B., Qin, Z., Shefelbine, S.J., Buehler, M.J., 2015. Influence of cross-link structure, density and mechanical properties in the mesoscale deformation mechanisms of collagen fibrils. J. Mech. Behav. Biomed. Mater. 52, 1–13.

Destrade, M., Horgan, C.O., Murphy, J.G., 2015. Dominant negative Poynting effect in simple shearing of soft tissues. J. Eng. Math. 95 (1), 87–98.

Eekhoff, J.D., Fang, F., Lake, S.P., 2018. Multiscale mechanical effects of native collagen cross-linking in tendon. Connect. Tissue Res. 59 (5), 410–422.

Eyre, D.R., Paz, M.A., Gallop, P.M., 1984. Cross-linking in collagen and elastin. Annu. Rev. Biochem. 53 (1), 717–748.

Fantner, G.E., Oroudjev, E., Schitter, G., Golde, L.S., Thurner, P., Finch, M.M., Turner, P., Gutsmann, T., Morse, D.E., Hansma, H., et al., 2006. Sacrificial bonds and hidden length: unraveling molecular mesostructures in tough materials. Biophys. J. 90 (4), 1411–1418.

Fratzl, P., 2008. In: Fratzl, P. (Ed.), Collagen. Structure and Mechanics. Springer.

Fujimoto, D., 1982. Aging and cross-linking in human aorta. Biochem. Biophys. Res. Commun. 109 (4), 1264–1269.

Gasser, T.C., Ogden, R.W., Holzapfel, G.A., 2006. Hyperelastic modelling of arterial layers with distributed collagen fibre orientations. J. R. Soc. 3, 15–35.
Gültekin, O., Dal, H., Holzapfel, G.A., 2019. On the quasi-incompressible finite element analysis of anisotropic hyperelastic materials. Comput. Mech. 63, 443–453.
Harrington, M.J., Gupta, H.S., Fratzl, P., Waite, J.H., 2009. Collagen insulated from tensile damage by domains that unfold reversibly: In situ X-ray investigation of mechanical yield and damage repair in the mussel byssus. J. Struct. Biol. 167 (1), 47–54.
Herod, T.W., Chambers, N.C., Veres, S.P., 2016. Collagen fibrils in functionally distinct tendons have differing structural responses to tendon rupture and fatigue loading. Acta Biomater. 42, 296–307.
Holzapfel, G.A., 2000. Nonlinear Solid Mechanics: A Continuum Approach for Engineering. John Wiley & Sons, Inc..
Holzapfel, G.A., Gasser, T.C., Ogden, R.W., 2000. A new constitutive framework for arterial wall mechanics and a comparative study of material models. J. Elasticity Phys. Sci. Solids 61 (1), 1–48.
Holzapfel, G.A., Ogden, R.W., 2020a. An arterial constitutive model accounting for collagen content and cross-linking. J. Mech. Phys. Solids 136, 103682.
Holzapfel, G.A., Ogden, R.W., 2020b. A damage model for collagen fibres with an application to collagenous soft tissues. Proc. R. Soc. Lond. Ser. A Math. Phys. Eng. Sci. 476 (2236), 20190821.
Horgan, C.O., Murphy, J.G., 2010. Simple shearing of incompressible and slightly compressible isotropic nonlinearly elastic materials. J. Elasticity 98 (2), 205–221.
Horgan, C.O., Murphy, J.G., 2011. On the normal stresses in simple shearing of fiber-reinforced nonlinearly elastic materials. J. Elasticity 104 (1), 343–355.
Horgan, C.O., Murphy, J.G., 2017. Poynting and reverse Poynting effects in soft materials. Soft Matter 13 (28), 4916–4923.
Janmey, P.A., McCormick, M.E., Rammensee, S., Leight, J.L., Georges, P.C., MacKintosh, F.C., 2007. Negative normal stress in semiflexible biopolymer gels. Nature Mater. 6 (1), 48–51.
Kang, H., Wen, Q., Janmey, P.A., Tang, J.X., Conti, E., MacKintosh, F.C., 2009. Nonlinear elasticity of stiff filament networks: strain stiffening, negative normal stress, and filament alignment in fibrin gels. J. Phys. Chem. B 113 (12), 3799–3805.
Kwansa, A.L., De Vita, R., Freeman, J.W., 2016. Tensile mechanical properties of collagen type I and its enzymatic crosslinks. Biophys. Chem. 214, 1–10.
Lin, S., Gu, L., 2015. Influence of crosslink density and stiffness on mechanical properties of type I collagen gel. Materials 8 (2), 551–560.
Mihai, L.A., Goriely, A., 2011. Positive or negative Poynting effect? The role of adscititious inequalities in hyperelastic materials. Proc. R. Soc. A 467 (2136), 3633–3646.
Mihai, L.A., Goriely, A., 2013. Numerical simulation of shear and the Poynting effects by the finite element method: an application of the generalised empirical inequalities in non-linear elasticity. Int. J. Non-Linear Mech. 49, 1–14.
Mikšík, I., Deyl, Z., 1991. Change in the amount of ϵ-hexosyllysine, UV absorbance, and fluorescence of collagen with age in different animal species. J. Gerontol. 46 (3), B111–B116.
Nolan, D.R., Gower, A.L., Destrade, M., Ogden, R.W., McGarry, J.P., 2014. A robust anisotropic hyperelastic formulation for the modelling of soft tissue. J. Mech. Behav. Biomed. Mater. 39, 48–60.
Ogden, R.W., 1997. Non-Linear Elastic Deformations. Dover, New York.
Ogden, R.W., Roxburgh, D.G., 1999. A pseudo–elastic model for the Mullins effect in filled rubber. Proc. R. Soc. Lond. Ser. A Math. Phys. Eng. Sci. 455 (1988), 2861–2877.
Poynting, J.H., 1909. On pressure perpendicular to the shear planes in finite pure shears, and on the lengthening of loaded wires when twisted. Proc. R. Soc. Lond. Ser. A 82 (557), 546–559.
Sáez, P., Peña, E., Martínez, M.A., 2014. A structural approach including the behavior of collagen cross-links to model patient-specific human carotid arteries. Ann. Biomed. Eng. 42 (6), 1158–1169.
Sansour, C., 2008. On the physical assumptions underlying the volumetric-isochoric split and the case of anisotropy. Eur. J. Mech. A Solids 27 (1), 28–39.
Shabbir, H., Dellago, C., Hartmann, M.A., 2019. A high coordination of cross-links is beneficial for the strength of cross-linked fibers. Biomimetics 4 (1), 12.
Simo, J.C., Taylor, R.L., Pister, K.S., 1985. Variational and projection methods for the volume constraint in finite deformation elasto-plasticity. Comput. Methods Appl. Mech. Engrg. 51 (1–3), 177–208.
Snedeker, J.G., Gautieri, A., 2014. The role of collagen crosslinks in ageing and diabetes – the good, the bad, and the ugly. Muscles Ligaments Tendons J. 4 (3), 303–308.
Spencer, A.J.M., 1971. Part III. Theory of invariants. In: Eringen, A.C. (Ed.), Continuum Physics, Volume I – Mathematics. Academic Press, New York, pp. 239–353.
Svensson, R.B., Mulder, H., Kovanen, V., Magnusson, S.P., 2013. Fracture mechanics of collagen fibrils: influence of natural cross-links. Biophys. J. 104 (11), 2476–2484.
Truesdell, C., Noll, W., 2004. In: Antman, S.S. (Ed.), The Non-Linear Field Theories of Mechanics. Springer-Verlag, Berlin, 3rd edition.
Uzel, S.G., Buehler, M.J., 2011. Molecular structure, mechanical behavior and failure mechanism of the C-terminal cross-link domain in type I collagen. J. Mech. Behav. Biomed. Mater. 4 (2), 153–161.
Willett, T.L., Labow, R.S., Aldous, I.G., Avery, N.C., Lee, J.M., 2010. Changes in collagen with aging maintain molecular stability after overload: evidence from an in vitro tendon model. J. Biomech. Eng. 132 (3), 031002.
Yoshida, K., Jiang, H., Kim, M., Vink, J., Cremers, S., Paik, D., Wapner, R., Mahendroo, M., Myers, K., 2014. Quantitative evaluation of collagen crosslinks and corresponding tensile mechanical properties in mouse cervical tissue during normal pregnancy. PLoS One 9 (11), e112391.
Žagar, G., Onck, P.R., Van Der Giessen, E., 2015. Two fundamental mechanisms govern the stiffening of cross-linked networks. Biophys. J. 108 (6), 1470–1479.
Zheng, Q.S., 1994. Theory of representations for tensor functions – a unified invariant approach to constitutive equations. Appl. Mech. Rev. 47, 545–587.
Zieman, S.J., Kass, D.A., 2004. Advanced glycation end product cross-linking: Pathophysiologic role and therapeutic target in cardiovascular disease. Congest. Heart Fail. 10 (3), 144–151.